NIST Technical Note 1787

Characterization of Airborne Nanoparticle Released from Consumer Products

Final Report to U.S. Consumer Product Safety Commission Interagency Agreement CPSC-I-12-0007

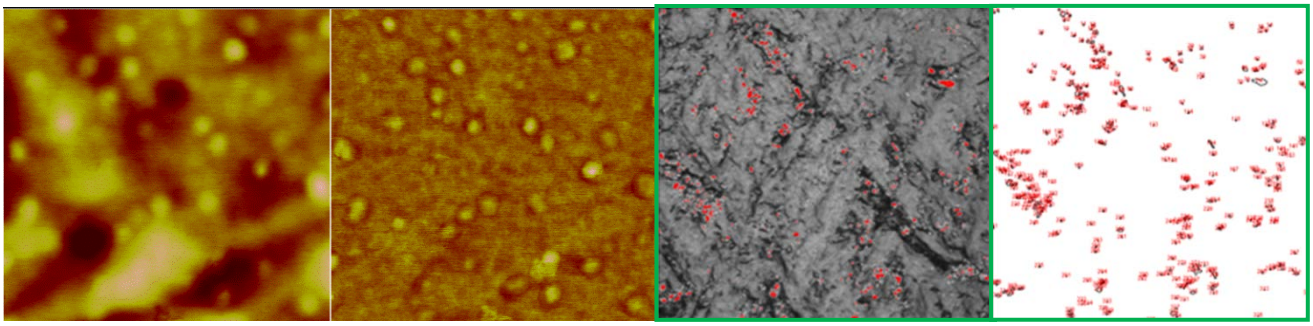

Tinh Nguyen
Lipiin Sung
Joannie Chin
Andrew Persily

http://dx.doi.org/10.6028/NIST.TN.1787
August 2013

National Institute of Standards and Technology
U.S. Department of Commerce

NIST Technical Note 1787

Characterization of Airborne Nanoparticle Released from Consumer Products

Final Report to U.S. Consumer Product Safety Commission Interagency Agreement CPSC-I-12-0007

Tinh Nguyen
Lipiin Sung
Joannie Chin

Materials and Structural systems Division
Engineering Laboratory

Andrew Persily

Materials and Structural systems Division
Engineering Laboratory

http://dx.doi.org/10.6028/NIST.TN.1787

August 2013

U.S. Department of Commerce
Rebecca Blank, Acting Secretary

National Institute of Standards and Technology
Patrick D. Gallagher, Under Secretary of Commerce for Standards and Technology and Director

National Institute of Standards and Technology Technical Note 1787
Natl. Inst. Stand. Technol. Tech. Note 1787, 47 pages (August 2013)
http://dx.doi.org/10.6028/NIST.TN.1787
CODEN: NTNOEF

Characterization of Airborne Nanoparticle Released from Consumer Products
Final Report to U.S. Consumer Product Safety Commission
Interagency Agreement CPSC-I-12-0007

Tinh Nguyen, Lipiin Sung, Joannie Chin, and Andrew Persily
Engineering Laboratory
National Institute of Standards and Technology
Gaithersburg, Maryland

Abstract

This report summarizes research results to date under the FY2012 interagency agreement between CPSC and NIST to develop testing and measurement protocols for determining the quantities and properties of nanoparticles released from flooring finishes and interior paints. This report includes: 1) a critical assessment of products, 2) literature review of nanoparticle release from nanocomposite coatings and paints by mechanical forces, 3) surface morphology characterization of nano-filled flooring coatings and interior paints before abrasion, 4) materials and experiment to evaluate the use of a Taber abraser for generating particles from flooring coatings and interior paints, 5) experimental protocols for abrasion test and analyses of release particles and abraded surfaces, 6) concentration, size distribution and chemical composition data for release nanoparticles accumulated on nano-filled coating and paint surfaces under different abrading conditions and wheel type, and 7) preliminary data on chemical composition of abraded nano-filled flooring coating and interior paint surfaces.

Table of Contents

Abstract…….
List of Figures……
List of Tables……..
1. Product Assessment ..... **1.**

1.1. Background ..... **1.**
1.2. Polymer-Inorganic Oxide Nanocomposites ..... **2.**
1.3 Polymer-CNT Nanocomposites ..... **3.**
1.4. Polymer-Clay Nanocomposites ..... **4.**

2. Literature Review of Nanoparticle Release from Polymer Nanocomposites by Mechanical Forces ..... **5.**
2.1 Background ..... **5.**
2.2. Previous Studies of Particle Release by Mechanical Forces ..... **7.**

3. Materials, Instrumentation, and Experimental Procedures ..... **9.**
3.1. Materials ..... **9.**
3.2 Sample Preparations ..... **12.**
3.3. Abrasion Instrumentation ..... **14.**
3.4. Abrasion Process ..... **15.**
3.5. Characterization of Surface Morphology and Mechanical Properties of Nano-filled Flooring Coatings and Interior Paints Before Abrasion. ..... **17.**
3.6. Characterization of Abrasion-induced Surface Release Particles and Abraded Surfaces. ..... **18.**
3.7. Experiment to Evaluate Laser Scanning Confocal Microscopy (LSCM) for Quantifying Abrasion-Induced Surface Release Particles. ..... **19.**

4. Results and Discussion ..... **21.**
4.1. Surface Morphology of Nano-filled Flooring Coatings and Interior Paints before Abrasion ..... **21.**
4.2 Mechanical Properties of Nano-filled Coated Wood Floor and Painted Drywall. ..... **26.**
4.3. Feasibility of LSCM for Quantifying Distribution of Mechanical-induced Release Particles on Nano-filled Flooring Coating and Paint Surfaces. ..... **26.**
4.4. Effects of Abrasion Parameters and Wheel Type on Release Particles Accumulating on the Nanocomposite Coating and Paint Surfaces ..... **32.**
4.4.1. Effects of Wheel ..... **32.**
4.4.2. Effects of Vacuum ..... **36.**
4.4.3. Effect of Abrasion Cycle and Applied Load ..... **38.**
4.5. Characterization of Surface Release Particles and Abraded Surfaces ..... **38.**
4.5.1. Characterization of Surface Release Particles ..... **38.**
4.5.2. Characterization of Abraded Surfaces ..... **42.**

5. Summary of Preliminary Findings and Further Studies ..... **43.**

6. References ..... **44.**

Acknowledgments ..... **47.**

List of Figures

Figure 1. Demands of polymer-metal oxide nanoparticle composites (1) ..... **3.**
Figure 2. Various mechanisms of particle release during life cycle of polymer nanocomposites and factors affecting the release rate. ..... **6.**
Figure 3. Six types of polymer nanocomposite coated flooring and painted panels used in this study. ..... **11.**
Figure 4. A schematic of steps used for obtaining the abraded discs having a diameter of 10 mm and a thickness of 0.7 mm from the 100 mm x 100 mm x 11mm painted drywall panels. ..... **13.**
Figure 5. a) A schematic of the 22 window aluminum holder, and b) a picture of the 22 window aluminum holder with the 10 mm diameter nano PU coated oakspecimens on it. ..... **13.**
Figure 6: Dual specimen Taber rotary abraser with a nano-filled PU coated wood flooring specimen. ..... **14.**
Figure 7. Picture of the duel-specimen Taber rotary abraser in the nano enclosure..... **15.**
Figure 8. LSCM imaging locations on an abraded coated flooring specimen..... **21.**
Figure 9a. LSCM images at 5x (upper row) and 150x (lower row) of unfilled and nano-filled PU flooring coatings on oak; a) unfilled PU, b) 1.0 % Al_2O_3 PU, and c) 3.0 % nanoSiO_2 PU..... **22.**
Figure 9b. LSCM images at 5x (upper row) and 150x (lower row) of control and nano-filled latex paints on drywall substrate; a) control, b) 1.2 % nanoTiO_2 paint, and c) 1.2 % nanoZnO paint. ..... **23.**
Figure 10a. Height and phase AFM images at different magnifications for unfilled and nano-filled PU flooring coatings. In each pair, height image is on the left and phase image is on the right. ..... **24.**
Figure 10b. Height and phase AFM images at different magnifications for control and nano-filled latex paints; The inset (bottom row, far right) is a typical 200 nm scan phase image of the 1.2 % TiO_2 paint, showing the latex microstructure. In each pair, height image is on the left and phase image is on the right. ..... **25.**
Figure 11. Pictures of several abraded nanoAl_2O_3–filled PU coated oak panels for different abrasion parameters, showing the loss of surface gloss in the abrasion area. ..... **27.**
Figure 12. Representative 150x LSCM images of abraded nanoAl_2O_3 PU flooring coating for two abrasion speeds and at two numbers of cycles..... **28.**
Figure 13. An example of analysis of LSCM images for abraded nano-filled PU flooring coating surfaces to obtain the total number and size distribution of surface release particles generated by abrasion. The abrasion parameters are speed 72 rpm (7.53 rad/s), loading 1000 g, and 500 cycles. Error bars represent one standard deviation..... **29.**
Figure 14. Effects of adhesive tape application on the number of particles and appearance of abraded nanoAl_2O_3 PU coating surface. Upper row: particle counts, LSCM images of abraded coating, and adhesive tape surfaces before the tape application; lower row: particle counts, LSCM images of abraded coating, and tape surfaces after the tape application. The image size is 56 μm x 56 μm, and the uncertainty for the particle count is <15 %..... **32.**
Figure 15. Effects of wheel type on the abraded surface characteristics and number of surface release particles for nanoAl_2O_3 PU coating. For each wheel type, a picture of the

abraded surface is on the left, LSCM image at 150x is in the middle, and number and size distribution of surface release particles is on the right. Abrasion parameters are speed 60 rpm (6.28 rad/s), loading 1000 g, and 100 cycles. Error bars represent one standard deviation..... **34.**

Figure 16. Effects of wheel type on the abraded surface characteristics and number of surface release particles for nanoTiO_2 latex paint. For each wheel type, a picture of the abraded surface is on the left, LSCM image at 150x is in the middle, and number and size distribution of surface release particles is on the right. Abrasion parameters are given in the bar plots. The insets in the pictures (far left on top and middle rows) are from control latex paint, showing a greater amount of green particles by the SC-17 wheel than the CS-10 wheel. Error bars represent one standard of deviation. ..... **35.**

Figure 17. Effect of vacuum on the number and size distribution of surface release particles; a) with a vacuum, and b) no vacuum. A CS-17 wheel was used, and the abrasion parameters are speed 60 rpm (6.28rad/s), loading 1000 g, and 100 cycles. Error bars represent one standard eviation.....**36.**

Figure 18. Effects of abrasion cycle and applied load on the number and size distribution of surface release particles for nanoAl_2O_3 PU coating (upper row), and nanoTiO_2 latex paint (lower row): a) 1000 g loading, and b) 500 g loading. A CS-10 wheel was used. Error bars represent one standard deviation. ..... **37.**

Figure 19. SEM images of surface release particles generated by the S-35 wheel for nano-filled PU flooring coatings, a) 3 % nanoSiO_2 PU, and b) 1 % nanoAl_2O_3. .....**39.**

Figure 20. SEM images of surface release particles generated by the S-35 wheel for nano-filled latex paint, a) 1.2% nanoZnO paint, and b) 1.2 % nanoTiO_2 paint..... **40.**

List of Tables

Table 1. Wheel types and their characteristics. ..... **16.**
Table 2. Parameters used for LSCM feasibility study. ..... **20.**
Table 3. Surface mechanical properties of PU flooring coating and latex paint with and without nanoparticles. ..... **26.**
Table 4. The number of particles for each size in a 56 µm x 56 µm abraded area on unfilled and nanoAl_2O_3-filled PU flooring coatings abraded at two speeds, three number of cycles, and a fixed 1000 g applied load. ..... **30.**
Table 5. ICP-MS results for surface release particles released from control and nano-filled flooring coatings and latex paints. ..... **42.**
Table 6. Elemental concentrations for abraded surfaces of control paint and nano-filled latex Paints. ..... **43.**

1. Product Assessment

1.1. Background

From wood and tar to today's synthetic plastics, polymers provide essential materials for a wide range of applications, including consumer products, construction, and transportation. Estimates of annual polymer production range from (120 to 180) billion kilograms (1). By adding fillers, pigments, and additives, a variety of polymeric materials with unique properties can be produced. Nanometer-size fillers (i.e., nanomaterials), such as spherical nanoparticles, layered platelets, tubes, and rods, have exceptional properties such as very high electrical conductivity, high mechanical strength, high surface area, and special electronic structures. Because many vital chemical and physical interactions are governed by surface properties, incorporating high surface area nanomaterials into a polymer can substantially change many properties of the host matrix. Experimental observations of large property enhancements achieved through a small addition (less than 5 mass %) of nanomaterials to polymer matrices have fueled intensive research over the past decade. This is strongly evidenced in recent reviews on polymer nanocomposites for a variety of nanomaterials (2-6).

Polymer nanocomposites differ from traditional plastic composites in that they provide greatly enhanced properties with a minimum effect on mass and without major processing modifications. In the past few years, polymer nanocomposite applications have gained a strong commercial footing, due to the outstanding performance of these advanced materials and the efforts of resin manufacturers and compounders who offer user-friendly products. In coming years, products based on nanotechnology will enter the consumer markets in large quantities. Due to the future potential of nanotechnology, many companies across the world are investing heavily in this sector. These advanced composites are increasingly used in essentially every segment of the industry from textiles and food packaging to buildings and construction, electronic products, and sporting goods. In 2006, about 300 commercial products on the market claimed to contain nanomaterials; this number had quadrupled by 2010 (7). Today, more than 1300 manufacturers have nano-enabled products in the commercial market around the world. According to the Nanotechnology Market Forecast to 2013 Report, the market for nano-manufactured goods will top 1.6 trillion US dollars in 2013, with an annual growth of more than 49 % between 2009 to 2013 (8). Although applications vary widely, polymer nanocomposites generally take advantages of exceptional nanomaterial properties such as mechanical enhancement, gas barrier, flame retardancy, thermal or electrical conductivity, and electronic

structure. Depending on the types of nanomaterials used, advantages of polymer nancomposites over traditional polymer products include their being stronger, harder, tougher, lighter, more dimensionally stable, less permeable, and more durable.

Because a variety of nanomaterials can be used to significantly improve the performance of polymer coatings, the coating nanotechnology (nano coatings) segment alone is projected to increase from $3.4 billion in 2010 to nearly $18 billion in 2015, an average increase of 39.5% (9), while the nano adhesive market is estimated to increase at 36.4%, from $257 million in 2010 to $1.2 billion in 2015. The main markets for polymer nanocomposite coatings are currently focused on easy-cleaning, self-cleaning, dirt resistant, impermeable, and scratch-resistant products. The fastest growing markets to 2016 will be interior and exterior coatings, which are driven by the increased demands for protective and repellent functions (10).

A variety of nanomaterials are being, or potentially will be, incorporated in polymer matrices for a wide range of applications. Because it would not be possible to go into great detail as to all nanomaterials for various applications, this product assessment only covers the three most common polymer nanocomposites used for consumer products, including paints and coatings, sporting goods, and electronics. They are polymer-metal oxides, polymer-carbon nanomaterials, and polymer-nanoclays. Although silver nanoparticles are the most common nanomaterials used in commercial nano-enabled products, this assessment does not include this material because it is mostly used in non-polymer nanocomposite products. Reference (7) provides a brief assessment of this nanomaterial.

1.2. Polymer-Inorganic Oxide Nanocomposites

Currently, metal oxide nanoparticles, such as alumina (Al_2O_3), titania (TiO_2) and nonmetal oxides, such as silicon dioxide (SiO_2), are the largest volume nanomaterials used for polymer nanocomposites (1). These metal oxide nanoparticles serve many functions in the plastics, coatings and electronics industries, as shown in Figure 1. TiO_2 and ZnO are traditionally used as pigments to enhance the appearance and improve the durability of polymeric products. However, due to their ability to absorb broad band ultraviolet (UV), these materials at nanosize have been exploited in many applications including self-cleaning coatings, UV-resistant coatings, sunscreens, and disinfectant sprays. These nanomaterials are also used for modifying optical properties, for example, increasing the refractive index of coatings. Due to their aid in surface cleaning, TiO_2 and ZnO nanoparticles are currently used in interior paints for kitchens and

bathrooms. The market for TiO_2 nanoparticles is projected to grow significantly the next five years, from $360 million in 2009 to $1.4 billion by 2017 (7).

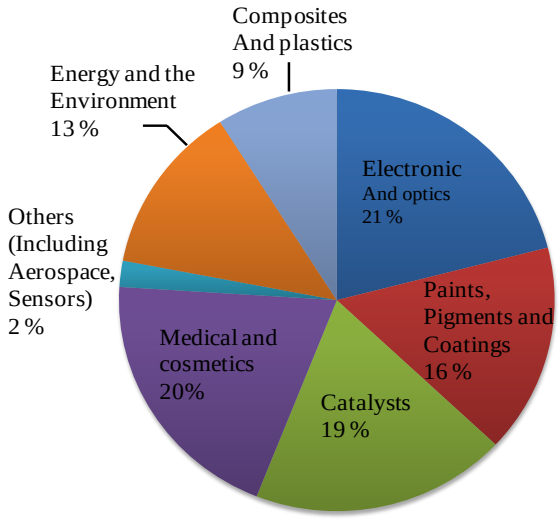

Figure 1. Demands of polymer-metal oxide nanoparticle composites (1).

Other metal oxide nanoparticles such as alumina and silica are currently added to polymer coatings, such as flooring coatings (i.e., finishes), to increase their scratch and abrasion resistance. A variety of commercial coatings and paints containing nanoparticles from a number of companies are currently available at paint stores and large hardware chains (1).

1.3 Polymer-CNT Nanocomposites

Carbon nanotubes (CNTs) are ideal nanomaterials for enhancing the performance of polymers where high strength, high thermal stability, exceptional electrical conductivity, and high aspect ratio can distinguish them from other nanomaterials. For this reason, polymer-CNT composites are being used or considered for use in a variety of applications, from consumer products to the aerospace industry. The CNTs that have been used in polymer nanocomposites are multi-walled nanotubes (MWNTs), which consist of several concentric graphene cylinders with the diameter ranging from 5 nm to 100 nm. MWCNTs have been incorporated in a variety of thermosets, such as epoxy and phenolic resins, and thermoplastic polymers, such as polypropylene and polyamide (nylon). Some of the current and potential applications of polymer-MWCNT nanocomposites in consumer products include paints and coatings, bicycle and tennis racquet frames, photovoltaic devices, hoses, baseball bats, and adhesives. Melt mixing, solution casting, and electrospinning are common methods employed for preparing

polymer-CNT composites. One important characteristic of CNTs is their strong van der Waals interactions, which cause them to form bundles and affects their dispersion in polymer matrices. Production of CNTs is projected to increase steadily, with a volume of 2916 tons in 2011 to 6750 tons for 2016. Approximately 35 % of the total CNT applications are polymer composites and coatings (1). Because of the exceptional strength, high friction, and ability to photostabilize polymers of the CNTs, polymer-MWCNTs composites will potentially be used for a variety of consumer products, such as exterior paints, decking, playgrounds, and coatings for decking.

1.4. Polymer-Clay Nanocomposites

Nanoclays used in polymer composites include natural clays, such as montmorillonite, and bentonite, and synthetic clays, such as laponite and magadiite. The main advantage of synthetic nanoclays is their chemical purity to provide transparent composite products. Because of their high surface area and surface reactivity, montmorillonite is the most widely used polymer nanocomposites today. Nanoclays have been incorporated in many common polymers including epoxies and polyurethanes. When properly dispersed in a polymer matrix, individual nm-thick clay layers become fully separated to form plate-like nanoparticles with very high aspect ratios. The presence of plate-like, high aspect ratio nanoclays will improve several properties of polymers including stiffness, strength, fire retardancy, gas permeability, and dimensional stability. For that reason, the main applications for polymer-clay nanocomposites today are for packaging materials. Nanoclays are also used as rheological modifiers in paints and inks. Other significant applications of polymer-clay nanocomposites are automotive and aerospace industries. Worldwide volume of nanoclays produced in 2012 is 9,070,000 kg (10,000 tons) with a projected volume of 13,423,500 kg (14,800 tons) in 2016. Forty percent of the demand is for automobile applications, 35 % for food packaging, and about 10 % in paints and coatings (1).

Other nanomaterials, such as carbon nanofibers, graphene, and fullerenes, have also been incorporated in polymer matrices for a variety of specialty applications. However, the demand volume for these nanomaterials at present is much less than the ones given above (1), and thus not covered in this section.

2. Literature Review of Nanoparticle Release from Polymer Nanocomposites by Mechanical Forces

2.1. Background

During their life cycles, polymer nanocomposites can be exposed to a variety of mechanical forces (e.g., abrasion, scratching, and washing) and harsh environments (e.g., UV radiation, temperature, and water). However, polymer matrices, being made up of organic molecules, have low resistance to mechanical stresses and are vulnerable to environmental attack. Under repeated mechanical and environmental stresses during service and post service, nanomaterials incorporated in a polymer matrix may be exposed on the nanocomposite surface and/or released from the host matrices. Because toxicological studies have shown that nanomaterials potentially pose environmental, health and safety (EHS) risks (12-17), there is an urgent need for risk assessment and guidelines to ensure the safe use and disposal of polymer nanocomposites. Further, public concern about the harmful effects of surface-exposure and release of nanomaterials during the life cycle of their polymer composites may present a roadblock to innovation and restrict the wide-spread use of these materials. While it may be possible that nanomaterials embedded in a polymer matrix will not be released to a significant extent, the release of hazardous materials from commercial products has been previously reported, e.g., lead from paint, asbestos from tiles, etc.

This section assesses the main mechanisms by which nanomaterials may be surface-exposed and released during the life cycle of polymer nanocomposites. Release is defined here as objects that are removed from the polymer nanocomposites, which include individual nanomaterials and nanomaterials. Imbedded in the polymer matrix. Further, unless specifically stated, the release mechanisms of interest in this discussion are focused on polymer nanocomposites used in consumer products, such as paint and coatings, sporting goods, and electronics. The release of nanomaterials from polymer nanocomposites used in other applications, such as aerospace, medical devices, automotive, etc., are not included in this review section.

Several studies have presented various possible accidental and incidental scenarios of nanomaterial release during the life cycle of nanocomposites used in construction, textiles and consumer products (17-19). In general, the release of nanomaterials from the polymer nanocomposites occurs not only during production of the nanocomposites, but also during their use, recycling, disposal, and incineration. The prevailing release routes may be different for

different applications. For consumer products, mechanical forces, recycling, and incineration of solid wastes could be the main release routes. For textiles, in addition to release by mechanical and matrix degradation mechanisms and their synergistic effects, recycled textiles undergo various mechanical, thermal and chemical treatments that could also release nanomaterials from the composite fibers. Figure 2 illustrates possible mechanisms by which nanomaterials could be released during the life cycle of a polymer nanocomposite and factors that affect the release rate. The release mechanisms include mechanical stresses, matrix degradation, chemical dissolution and fire/incineration. Although the extent of release may be different at different stages of their respective life cycles, these scenarios should be generally applicable to other fields, such as aerospace, tires, and automobiles. As such, it can be expected that some fraction of nanomaterials that have been incorporated in the polymer matrix will be eventually released into the environment during a product's life cycle. Further, in addition to release, these various mechanisms could also expose nanomaterials on the nanocomposite surface. Therefore, risk assessment and risk management should deal with both the release of nanomaterials and their exposure on the composite surfaces.

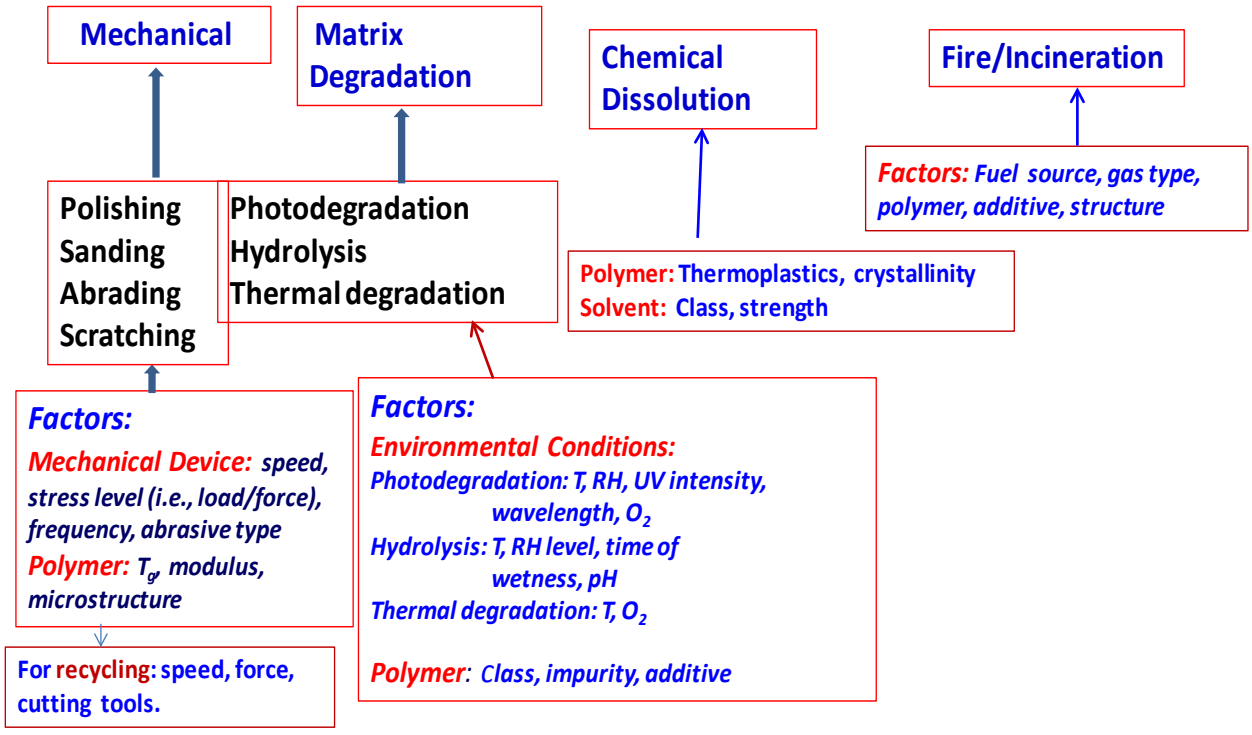

Figure 2. Various mechanisms of particle release during life cycle of polymer nanocomposites and factors affecting the release rate.

2.2. Previous Studies of Particle Release by Mechanical Forces

A variety of mechanical forces, such as abrading, polishing, sanding, sawing, drilling, and scratching, may cause a release of nanomaterials from the polymer matrices. A number of studies have employed mechanical abrasion devices to investigate the release of particles into the air (i.e., airborne particle release) from polymer nanocomposites and related nano-products. Because of the potential hazard of high aspect ratio, fibrous CNTs, several studies on the release of these nanocarbon materials have been reported. For example, Wohlleben et al. (20) investigated particle release due to sanding and abrasion of polyoxymethylene (POM)/5 % mass MWCNT and cement/4% mass MWCNT composites. The sanding and abrading represent typical homeowner repair practice and mechanical actions (e.g., shoes scuffing, chair movement, etc.), respectively, on coated flooring surfaces. The sanding was performed using a P320 grain size paper, while the abrasion was conducted using a Taber rotary abraser. The released particles were characterized by a variety of spectroscopic, microscopic, and size-measurement techniques for particles generated in the air. No difference was observed in the amounts of mechanical-induced release particles between matrices with and without MWCNTs, and that no free MWCNTs were detected for both POM and cement/MWCNT nanocomposites. Further, there was no evidence of CNT presence at the surface of the particles generated by sanding of polymer nanocomposites, but CNTs were observed on the surface of the sanded particles of the cement nanocomposites.

Schlagenhauf et al. (21) also employed the Taber rotary abraser and silica/alumina abrasive wheels to study the release of particles from an epoxy containing three different MWCNT loadings. Particles released in the air and collected on grids were analyzed. Four different modes of particle size distribution were observed, with the smallest size mode between 300 nm and 400 nm, and the other three modes containing particle sizes between 0.6 μm and 2.5 μm. Some particles from the abrasive wheels themselves were observed in the release particles, but the amount was small and did not affect the overall results. One particular finding of this study is that protruding, free standing, and aggregated CNTs were observed in the released particles. Based on this result, the authors recommended safety precautions be taken during mechanical processing of epoxy/MWCNTs composites.

A linear Taber abraser with a steel brush abrasive was employed by Golanski et al. (22) to study the airborne release of particles from polycarbonate (PC) containing 3 % mass CNTs and poly(methyl methacrylate)/10 % mass nanoCu composites. All operations were conducted in

a glove box, and abrasion variables included speed and applied load. A PC/MWCNT composite was found to release more particles having nanometer dimensions than a CNT-free PC. The size of released particles was between 10 nm and 6 μm. Further, the amounts of particles released in the air increased with increasing speed and applied load. No evidence of free MWCNTs was observed for released particles generated by the steel brush. However, when sanding paper was used as an abrasive, these authors reported the presence of free Cu nanoparticles released from poly(methyl methacrylate)/nanoCu composite. Although the types of the abrasive and other abrading parameters need to be investigated further, the results of this study suggested that the Taber abraser is suitable for generating particles from polymer nanocomposites for physical and chemical characterization and for toxicity studies.

Bello et al. (23) investigated airborne particles released during wet and dry machining of carbon fiber-epoxy and alumina fiber-epoxy composites containing MWCNTs. These advanced nano-enabled composites are being or will potentially be used in consumer products, such as in tennis racket frames and golf clubs. The volume fraction of MWCNTs in the carbon fiber composite was 0.05 % and that in alumina fiber composite varied between 0.5 and 4.5 %. Dry cutting used a band saw and wet cutting employed a rotary wheel with water flushing. Wet cutting did not produce particles significantly different with the background, but dry cutting produced large numbers of particles. However, the release levels, size distributions, and surface areas of released particles were not significantly different for composites with or without MWCNTs. Further, CNTs, either individual or in bundles, were not observed in all collected samples imaged with TEM or SEM. The same epoxy and alumina based composites, with and without MWCNT, were analyzed for particle release during drilling using abrasive, solid-core drill bits (24). In comparison to cutting, airborne particles generated by drilling were multi-modal having sizes ranging from 20 nm to 0.8 μm. The thickness of the composite was an important factor on the number of particles generated during cutting, but had less effect on drilling.

Particle release by mechanical forces has also been studied for polymeric materials containing other types of nanoparticle, including ZnO, Fe_2O_3 (25, 26), TiO_2 (27), and nanoclays (28). Gohler et al. (25) studied the particles released from polymer coatings containing ZnO and Fe_2O_3 using a mini sander. They noted that a substantial number of particles were released in the air but there was no difference in the number or size distribution of particles between coatings containing or not containing nanoparticles. Vorbau et al. (26) used a Taber abraser to assess the

particle release from several polymer coatings containing ZnO nanoparticles. Although the Taber abraser was found suitable for reproducibly releasing particles from nanocomposite coatings, the results showed no evidence of nanosize particles being generated. A Taber abraser was also employed by Golanski et al. (27) to abrade in liquid for paints containing TiO_2 nanoparticles. Submicroscopic and microscopic particles were released but no nanosize materials were detected. Airborne release particles generated by drilling of polymer amide-clay nanocomposites were studied by Sachse et al. (28). The number of release particles from the clay nanocomposite was reported to be 20 times lower than that for the same matrix without nanoclays. These authors suggested that the presence of nanoclay somehow discourages the formation of airborne particles.

In summary, mechanical forces can cause a substantial release of particles from polymer nanocomposites used in a variety of consumer products. Taber abrasers, linear or rotary, are generally utilized as a useful mechanical device to generate particles for analyses. Scanning mobility analyzers are commonly used to measure airborne particles and a nanoaerosol sampler is employed to collect released particles on TEM grids for morphological and chemical analyses. The number and size distribution of release particles depend on many factors, including mechanical methods used to generate particles, mechanical force speed, number of cycles, applied load, abrasive material, and polymer class and properties. Except for CNTs where bundles of MWCNTs have been observed on released particles for a few cases, most studies reported that nanoparticles are still imbedded in the released particles. More studies are needed to carefully characterize the release entities as a function of instrument parameters and material properties.

Literature on nanomaterial release by other mechanisms, such as matrix degradation by photoreaction, hydrolysis, and thermal treatment, polymer dissolution, and incineration, is not covered here. Reference (29) provides a brief review on these subjects for polymer-CNT composites.

3. Materials, Instrumentation, and Experimental Procedures**

3.1. Materials

A commercial water-based polyurethane (PU) flooring coating (finish and coating are used interchangeably in this report) and a commercial water-based latex interior paint were chosen for this study. The PU was a typical unfilled (clear) polymer coating used for hardwood

flooring, while the latex paint was a typical interior wall paint containing 30 % (based on mass of the polymer matrix) nepheline syenite tint base (aluminum silicate filler). The size of the nepheline syenite tint base particles is between 5 to 10 micrometers. Panels of unfilled PU coating, and Al_2O_3 and SiO_2 nanoparticle-filled PU coatings, latex paint containing no nanoparticles (control paint), and TiO_2 and ZnO nanoparticle-filled latex paints were prepared, cured, cut to desired size panels, and purchased by NIST from a commercial source. According to the material supplier, the diameter of Al_2O_3, SiO_2, TiO_2 and ZnO nanoparticles were 20 nm, 20 nm, 30 nm, and 40 nm, respectively. Al_2O_3 and SiO_2 nanoparticles are commonly incorporated in PU coatings to increase the scratch and wear resistance of flooring finishes, and TiO_2 and ZnO nanoparticles are used in interior paints for ease in cleaning painted surfaces, most often in kitchens and bathrooms. Except for the generic names and nanoparticle loadings and size, information about chemical composition and physical properties of the PU flooring coating and interior latex paint is not available. Note that only one flooring coating containing Al_2O_3 nanoparticles and one interior paint containing nanoTiO_2 nanoparticles were proposed to be studied in the first year. However, because the number of particles released by abrasion depends on material properties, other nanoparticles (i.e., SiO_2 for flooring coatings and ZnO for interior paint) are also included for this investigation. Further, in order to support the interpretation of data on the abrasion-induced release particles containing the incorporated nanoparticles, PU flooring coating and interior latex paint in the absence of nanoparticles (controls) are also included in this study.

According to the material supplier, unfilled and nano-filled PU flooring coatings were applied by brush on an oak wood substrate and consisted of four separate layers (four coats). Each layer was allowed to air dry for 8 hours before the next layer was applied. This procedure is typical for water-based coating products sold in the consumer market for flooring finishes. The oak substrate was a solid wood material having a thickness of 6.25 mm (1/4 inch). The substrate was an one-piece or multiple 25 mm wide strip material. The control and nano-filled latex paints were applied on a drywall substrate by roller and consisted of four layers with 4 hours of air drying time between the layer applications. The drywall was a composite assembly having a thickness of 11 mm (7/16 inch), which consists of a 10 mm thick powdery gypsum board sandwiched between two 0.5 mm thick paper boards.

A total of 192 100 x 100 mm (4 inch x 4 inch) panels of nano-filled flooring coatings and nano-filled interior paints and their controls were purchased for this study. Their characteristics are given below.

1. 32 panels of 100 mm x 100 mm unfilled PU coating on oak substrate (control PU flooring coating).
2. 64 panels of 100 mm x 100 PU coating containing 1.0 % nanoAl_2O_3 on oak substrate (designated as nanoAl_2O_3 PU); two batches of panels were prepared and supplied at two different times.
3. 32 panels of 100 mm x 100 mm PU coating containing 3 % nanoSiO_2 on oak substrate (nanoSiO_2PU).
4. 32 panels of 100 mm x 100 mm latex paint on drywall (control paint). Note that the control latex paint as supplied contained a 30 % by mass of aluminum silicate filler, as noted above.
5. 32 panels of 100 mm x 100 mm latex paint containing 1.2 % nanoTiO_2 on drywall substrate (nanoTiO_2 paint).
6. 32 panels of 100 mm x 100 mm latex paint containing 1.2 % nanoZnO on drywall substrate (nanoZnO paint).

Figure 3 displays six types of panels used in this study.

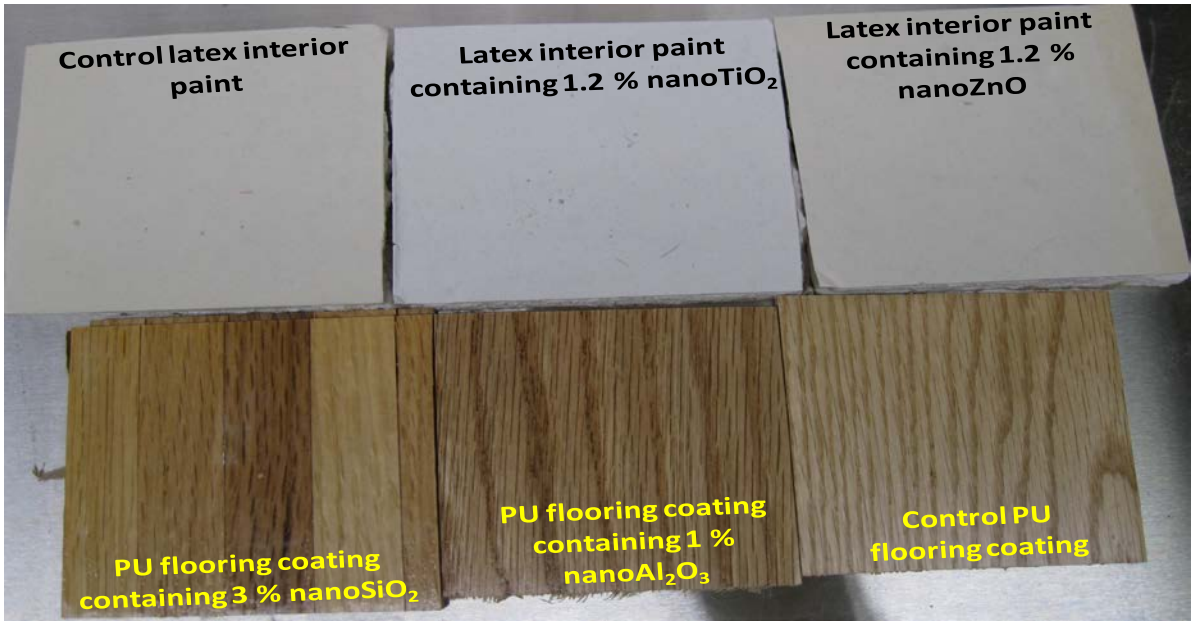

Figure 3. Six types of polymer nanocomposite coated flooring and painted panels used in this study.

3.2. Specimen Preparations

Two types of specimens were used for the abrasion experiments of nano-filled flooring coatings and nano-filled interior paints. The first type was used as-received (i.e., ≈ 100 mm x 100 mm panels) for measuring the amounts and distribution of particles generated by the abraser. The 100 mm x 100 mm dimension is specified by the ASTM Standard Test Method D 4060-10 for evaluating the abrasion resistance of polymer coated surfaces. The second type of specimen was prepared as described below for characterization of the chemical composition and morphology of abraded surfaces and release particles generated by abrasion that are accumulated on the specimen surfaces using various analytical techniques. For these measurements, abraded specimens having appropriate dimension are imaged without any possible surface contamination that may occur after the abrasion process. Such contamination, particularly any additional particle deposition from the sample preparation or manipulation, will complicate the interpretation of the results. To achieve this objective, 10 mm diameter discs of nano-filled latex painted drywall and nano-filled PU coated oak were used. Because the mechanical properties and the construction of the wood and drywall substrates were markedly dissimilar, two different approaches were taken for preparing the 10 mm diameter discs from nanocomposite coated and latex painted panels.

For nano-filled interior paints, the steps for obtaining 10 mm diameter discs from the painted drywall panels are schematically shown in Figure 4. The painted paper board sides of several 100 mm x 100 mm x 11 mm dry wall panels were cut and then filed using a band saw to produce gypsum-free, flat painted paper sheets having a thickness of approximately 0.7 mm. The 100 mm x 100 mm x 0.7 mm painted paper sheets were then attached to 3 mm thick balsa wood veneers (0.16 g/cm^3 density) that have the same dimension. After abrading (using the same parameters as those for the 100 mm x 100 mm x 11 mm painted drywall panels), 10 mm diameter painted paper discs were punched from the abraded areas using a hardened steel core borer. Care was taken to minimize contamination of the abraded disc surfaces.

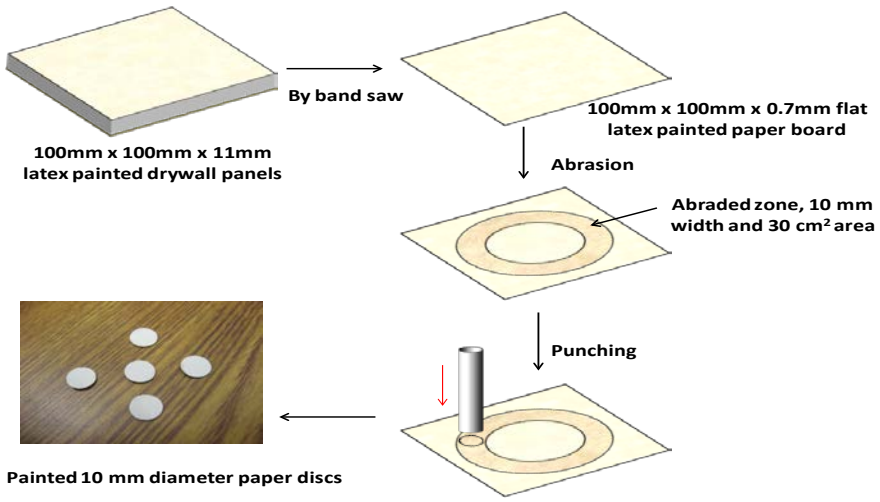

Figure 4. A schematic of steps used for obtaining the abraded discs having a diameter of 10 mm and a thickness of 0.7 mm from the 100 mm x 100 mm x 11mm painted drywall panels.

For nano-filled flooring coatings, coated wood discs having a diameter of 10 mm and a thickness of 2 mm fitting tightly in a 22 window aluminum holder were used for the abrasion (Figure 5a). The rim of each 10 mm diameter window of the aluminum holder was scored to facilitate the removal of each specimen. Disc specimens having a 10 mm diameter and 2 mm thickness were obtained by first thinning the 100 mm x 100 mm x 6.25 mm thick wood panels to 2 mm thick sheets. The 10 mm diameter discs (see Figure 5b) were then punched from these sheets using a hole saw. The 10 mm diameter discs on the aluminum holder were abraded using the tungsten carbide wheel, and the abraded discs were removed from the holder for analyses.

a b

Figure 5. a) A schematic of the 22 window aluminum holder, and b) a picture of the 22 window aluminum holder with the 10 mm diameter nano PU coated oak specimens on it.

3.3. Abrasion Instrumentation

This study used a dual specimen table Taber rotary abraser (Model 5155, Taber, North Tonawanda, NY) (Figure 6) that can abrade two specimens simultaneously. The Taber abraser is employed because it is widely used to evaluate the abrasion, wear, and rubbing resistance of coatings and paints and is specified in various international standards, including ASTM D 4060-95:2007, ISO 5470-1999, and DIN 68861-2-1981. This instrument has also been employed by various researchers involved in studies of nanoparticle releases from polymer nanocomposites due to mechanical forces such as abrasion, sanding, polishing, and chipping (21,22,26,27). The stress exerted by the Taber test simulates the typical mechanical stresses applied to organic coatings and paints, such as walking, chair movement, sanding, polishing actions, and rubbing. The Taber abraser consists of two abrasive wheels that abrade the material continuously while the specimen is rotating on a vertical axis at a fixed speed. The abrasion/rubbing action is produced by the friction at the contact line between the material and the sliding rotation of the two wheels.

Figure 6: Dual specimen Taber rotary abraser with a nano-filled PU coated wood flooring specimen.

The dual specimen table Taber abraser 5155 has a number of important features that facilitate the standardization of particle release study by abrasion. They include: 1) An easy-to-use operator interface that includes palpable feel buttons and a four-line digital display, 2) simple on-screen instructions that allow the operator to change the test parameters, 3) an internal memory to store the settings, 4) a precision vacuum nozzle adjustment that allows the height to be modified for accommodating varying specimen thickness, 5) a quick release mounting hub allowing quick wheel mounting, and 6) ease of changing the normal force.

3.4. Abrasion Process

The abrasion was performed in a 1.5 m x 0.725 m (60 inch x 29 inch) XPert® Nano Enclosure (LABCONCO, model 3887561), shown in Figure 7. The nano enclosure is equipped with an ULPA exhaust filter that can trap 120 nm particles at 99.999 % efficiency. It contains a built-in ionizer that neutralizes static charge on interior surfaces, which helps reduce powders being attracted to surfaces.

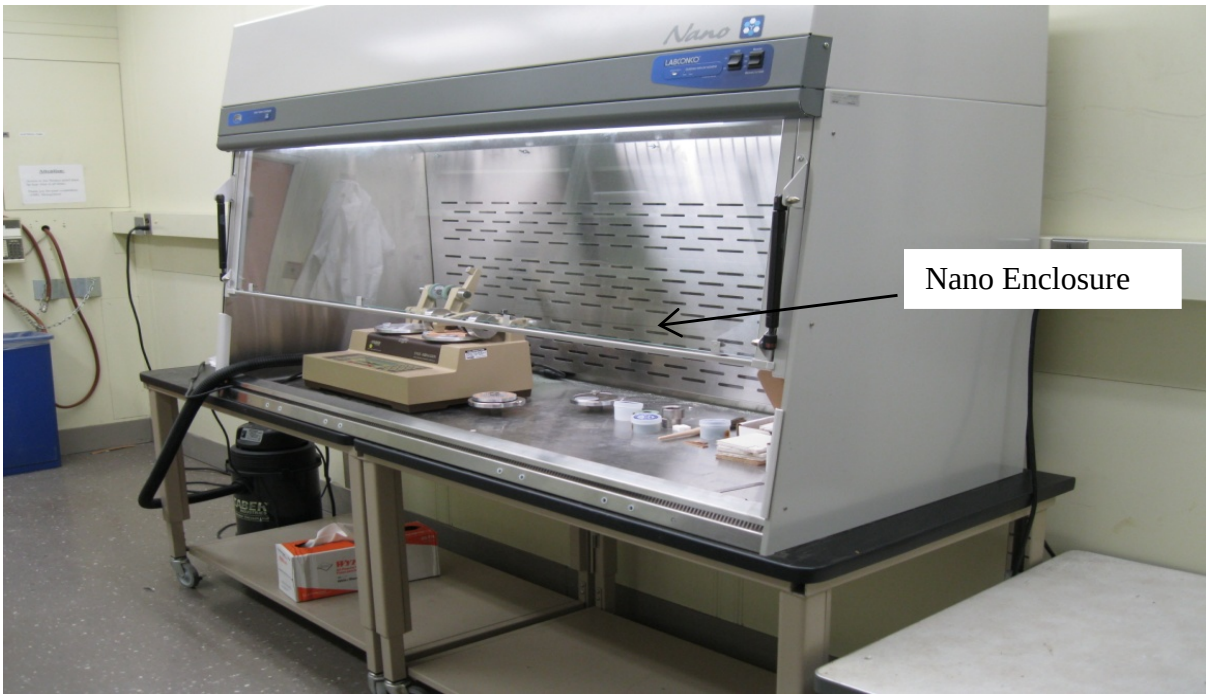

Figure 7. Picture of the duel-specimen Taber rotary abraser in the nano enclosure.

The abrasion testing involves mounting a flat specimen approximately 100 mm square, as shown in Figure 3, or round, on the turntable platform. A square specimen accessory was used in this study for abrading 100 mm x 100 mm PU coated and painted panels. The abraded zone forms a circular band having a 10 mm width and a surface area approximately 30 cm^2. In typical abrasion studies, the abrasion or wear resistance of a polymer coating is determined by measuring the specimen mass before and after abrasion. To provide data for developing a protocol for generating airborne particles and particles accumulated on the surface using an abrasion apparatus, a number of parameters were investigated, including abrasion speed, abrasion cycles, loading (force), vacuum (presence or absence), and wheel types. Because the amount of coating or paint removed from sample depends on the abrasive material of the wheel, three different wheel types having different abrasive materials and abrasion characteristics were selected, as shown in Table 1. CS-10 and CS-17 wheels are specified in ASTM 4060-10 for studying the abrasion resistance of organic coatings and have been used in several previous studies for generating airborne particles from polymer nanocomposites (26,27). Although they are recommended by the ASTM standard, the CS-10 and CS-17 wheels, which are made of rubber-abrasives, produce their own particles during abrasion. This would complicate the quantification and interpretation of particles released from the specimens. The wheel S-35 is made of a hard tungsten carbide material and is free of soft polymer matrix, which should greatly reduce the possibility of generating its own particles.

Table 1. Wheel types and their characteristics

Wheel Type	Composition	Abrasive action	Recommended Uses
CS-10	Rubber and alumina abrasive particles	Mild	Abrasion resistance of organic coatings according to ASTM D4060 – 10, 2007.
CS-17	Rubber and alumina abrasive particles	Harsh	Abrasion resistance of organic coatings according to ASTM D4060 – 10, 2007.
S-35	Tungsten Carbide	Severe	Resilient materials, e.g., flooring covering, rubber, etc.

3.5. Characterization of Surface Morphology and Mechanical Properties of Nano-filled Flooring Coatings and Interior Paints Before Abrasion

Surface morphology of nano-filled PU flooring coatings and nano-filled latex paints were characterized by laser scanning confocal microscopy (LSCM) and atomic force microscopy (AFM), and their mechanical properties were measured by a nanoindenter. In addition to measurement of surface morphology of specimens before abrasion, LSCM is also the main technique used in this study for quantifying the number and size distributions of particles accumulated on the specimen surface following the abrasion process. Because LSCM is not a common instrument for nanotechnology measurement, a brief description of this optical microscopy technique is provided here. More detailed description of LSCM can be found elsewhere (30).

LSCM utilizes coherent light and collects light exclusively from a single plane and rejects light out of the focal plane. By moving the focal plane, single images (optical slices) can be combined to build up a three dimensional stack of images that can be digitally processed. A two-dimensional (2D) LSCM projection image in the xy plane (512 pixel × 512 pixel) is formed by summing the stacks of the image in the z direction of the sample. Pixel intensity level represents the total amount of backscattered light. Brighter areas in an LSCM image represent regions that scatter more light than darker areas. The wavelength, numerical aperture of the objective, and the size of the pinhole dictate the resolution. LSCM can cover a wide range of length scale, from a surface area as large as 2.6 mm x 2.6 mm down to 20 μm x 20 μm by using different objectives of the instrument. It is a fast microscopic technique suitable for imaging particles and their clusters on a specimen surface. When combined with imaging analysis, LSCM can provide quantitative information on the number and distributions of particles having sizes ranging from 80 nm to 10 micrometers. In this study, LSCM was performed using a Zeiss model LSM510 and a laser wavelength of 543 nm. The images were taken at magnifications of 150x, with optical slice (*z*-step) of 0.1 μm. LSCM graphs reported in this report are 2D projection images, and 3D rendering images using Zeiss confocal software. The freeware *ImageJ* [31] was used with LSCM imaging to obtain data on size distribution of release particles and their agglomerates on the specimen surface.

AFM is a powerful technique for studying features and structures of material surfaces at a nanoscale spatial resolution. This instrument can help to identify individual nanoparticles on a specimen surface before and after abrasion. AFM measurements were carried out at ambient

conditions (24 ^{o}C, 50 % relative humidity) using a Dimension 3100 system (Veeco Metrology) and silicon probes (TESP 70, Veeco Metrology). Both topographic (height) and phase images were obtained simultaneously using a resonance frequency of approximately 300 kHz for the probe oscillation and a free-oscillation amplitude of 62 nm ± 2 nm.

Surface elastic modulus (E) and hardness (H) of nano-filled PU flooring coatings and nano-filled latex paints and their controls were measured using a NanoXP depth sensing instrument or nanoindenter (Agilent Technologies). The instrument is equipped with a 10 µm radius 45^{o} semi-apical angle diamond cone indenter. The nanoindentation experiment was conducted using a continuous stiffness mode at a fixed strain rate of 0.05 s^{-1} and indented to a depth of 3 µm. Reported modulus values are the average obtained between the depths of 1000 nm and 2000 nm for a minimum of 15 indents. Error bars represent one standard deviation from 15 measurements.

3.6. Characterization of Abrasion-induced Surface Release Particles and Abraded Surfaces

Two kinds of particles are generated during the abrasion of a material. One type is particles in the air, hereafter referred to as abrasion-induced airborne release particles or airborne release particles. The other type is particles accumulated on the specimen surface following the abrasion, hereafter referred to as abrasion-induced surface release particles or surface release particles. The measurement of abrasion-induced airborne release particles is being investigated separately. The characterization of surface release particles and abraded surfaces has been carried out and is reported here. These particles were characterized by LSCM, transmission electron microscopy (TEM), AFM, scanning electron microscopy (SEM), X-ray photoelectron spectroscopy (XPS), and inductively-coupled plasma mass spectrometry (ICP-MS). Information about the LSCM instrument and procedure is given above.

The SEM images were acquired using an FEI Helios NanoLab 650 Focused Ion Beam Scanning Electron Microscope. Secondary and backscattered detector electron images were collected using a through the lens detector in immersion mode. 2 keV to 5 keV electron beam energy, 100 pA beam current and 3 mm and 4 mm working distances were used. Particles generated from four materials using the S-35 wheel were characterized: nanoZnO paint, nanoTiO_2 paint, nanoSiO_2 PU coating, and nanoAl_2O_3 PU coating.

X-ray photoelectron spectroscopy (XPS), which provides chemical information on material surface, was performed using a Kratos Axis Ultra DLD (Chestnutridge, NY)

spectrophotometer using a monochromatic Al Kα X-ray source operating at 150 W with an energy of 1486.6 eV under ultra-high vacuum conditions (P_{base} = 8 x 10^{-8} Pa). 10 mm diameter disc specimens of nano PU coatings and nano latex paints were used for this measurement. Each specimen was initially pumped down overnight to remove any adsorbed water prior to analysis. The acquired spectra were analyzed with CasaXPS software (Teignmouth, UK) for elemental percent composition using one Shirley background fitting for each region with the exception of Zn which required 2 for each peak after referencing all energies to the hydrocarbon component of the C (1s) spectra at 284.5 eV.

The ICP-mass spectroscopy (ICP-MS) measurement of abrasion-induced surface release particles were conducted using the SemiQuant mode of Agilent model 7500cs. The SemiQuant mode is capable of quantifying elements of the entire periodic table by using the spectral information of the elements. The instrument was calibrated using a solution containing 20 μg kg^{-1} of each of 31 elements prepared by diluting ICP–MS Calibration Standard (Cat# ICP–MSCS) from High Purity Standards with 1.5 % HNO_3. NIST SRM 1643e Trace Elements in Water was used for quality assurance. For this measurement, surface release particles generated from a particular set of abrasion parameters were placed in a polyethylene bottle containing 25 ml of ion-free water. Each liquid sample contained a certain amount of precipitates at the bottom of the bottle. Because large particles (> 80 μm) cannot pass through the capillary of the sample introduction device, each sample was decanted to remove the precipitate. If free nanoparticles are present in the solution, they were expected to remain in the supernatant due to Brownian motion. Eight collected samples were analyzed for elements in the surface release particles, five of that were abraded with the CS-10 wheel and three were abraded with the S-35 wheel.

3.7. Evaluating LSCM Technique for Quantifying Abrasion-Induced Surface Release Particles

Well-established techniques, such as scanning mobility particle sizer (SMPS) and condensation particle counter (CPC), have been used to quantify airborne release particles resulting from mechanical actions, such as sanding, abrasion, and polishing (20-28). However, studies of release particles that accumulate on a material surface following mechanical force applications has not been reported, and there is essentially no information on the appropriate technique to effectively quantify this kind of particles. For that reason, an investigation was carried out to evaluate the feasibility of using the LSCM technique to quantify the number and size distribution of particles present on nano-filled coated and painted surfaces following an

abrasion. Although LSCM does not have the spatial resolution of an electron or scanning probe microscopy, it has several attributes that may be suitable for this application: fast, non-contact, non-destructive, and can be operated at ambient environmental condition. In addition to providing images of particles having different length scales from approximately 60 nm to 10 μm. LSCM can also yield 3D information, which helps to distinguish particles imbedded in the polymer matrix or loosely lying on the surface. Further, previous studies indicated that particles released in the air by the mechanical forces mostly have sizes greater than 100 nm. Therefore, the lack of a nanoscale resolution (i.e., < 80 nm) is not regarded as important for this application.

The LSCM instrumentation and procedure used to obtain size distribution of surface release particles for this investigation is given above. Only unfilled PU flooring and 1% Al_2O_3 – filled PU coatings were employed for this portion of the investigation. A CS-10 wheel was used in combination with a vacuum system to produce surface release particles. All abrasion operations were carried out at a fixed loading at 1000 g. To provide adequate data for assessing the suitability of LSCM for this purpose, the number of abrasion cycles and wheel speed were varied, as shown in Table 2.

Table 2. Parameters used for LSCM feasibility study

Speed: rad/s rpm*	6.28 60	6.28 60	6.28 60	7.53 72	7.53 72	7.53 72
# of Cycles	100	200	500	100	200	500

** For general practice in the abrasion processing, a non-SI unit of speed -rpm is used. So a non-SI unit of rpm is also used in this report for future comparison with other experiments done in the industrial laboratories.*

For each combination of speed and number of cycles, 16 LSCM images were collected from different locations of the abraded surface, as shown in Figure 8. This sampling will provide essential data to determine the variability of surface release particles within the 10 mm wheel width and 30 cm^2 abraded area.

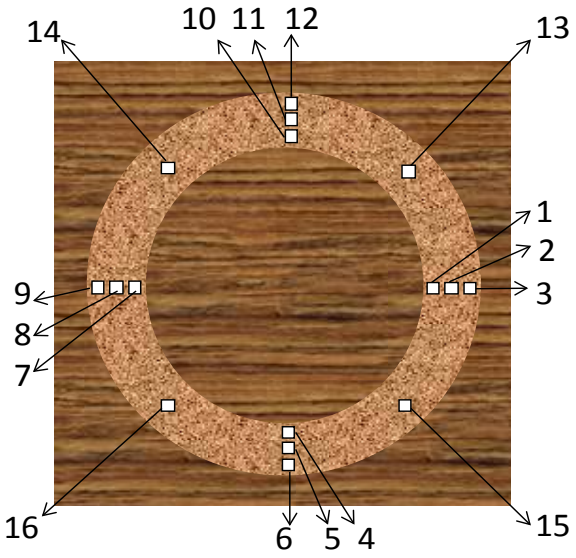

Figure 8. LSCM imaging locations on an abraded coated flooring specimen.

4. Results and Discussion

4.1. Surface Morphology of Nano-filled Flooring Coatings and Interior Paints before Abrasion

Representative LSCM images at two magnifications for control and nano-filled PU flooring coatings on oak substrate are illustrated in Figure 9a. At low magnification, the surface of the unfilled or 1 % nanoAl_2O_3–filled PU coating (top row, left and middle) shows heterogeneous features consisting of dark and bright regions, which is due to differences in surface topography of the specimen. The roughness (root mean square) of these surfaces was approximately 10 µm ± 2 µm. The surface of the 3 % nanoSiO_2–filled PU coating is smoother (top row, right), having a roughness of 2.2 µm ± 1 µm. A similar smooth surface is observed for control PU coating at 150x magnification. However, some particles or clusters of nanoparticles are observed on the surface of nanoSiO_2 and nanoAl_2O_3–filled PU coatings when imaged at the high magnification (150x). Without chemical identification, it is not certain whether these particles are from the incorporated nanoparticles near the specimen surface or due to dust from the air or from the specimen cutting. Although care was taken to blow off all debris from the specimen surface before LSCM imaging, it may be unavoidable that some debris generated during the sawing (to obtain the 100 mm x 100 mm panels) may adhere rather strongly to the surface and not be removed by the air blowing.

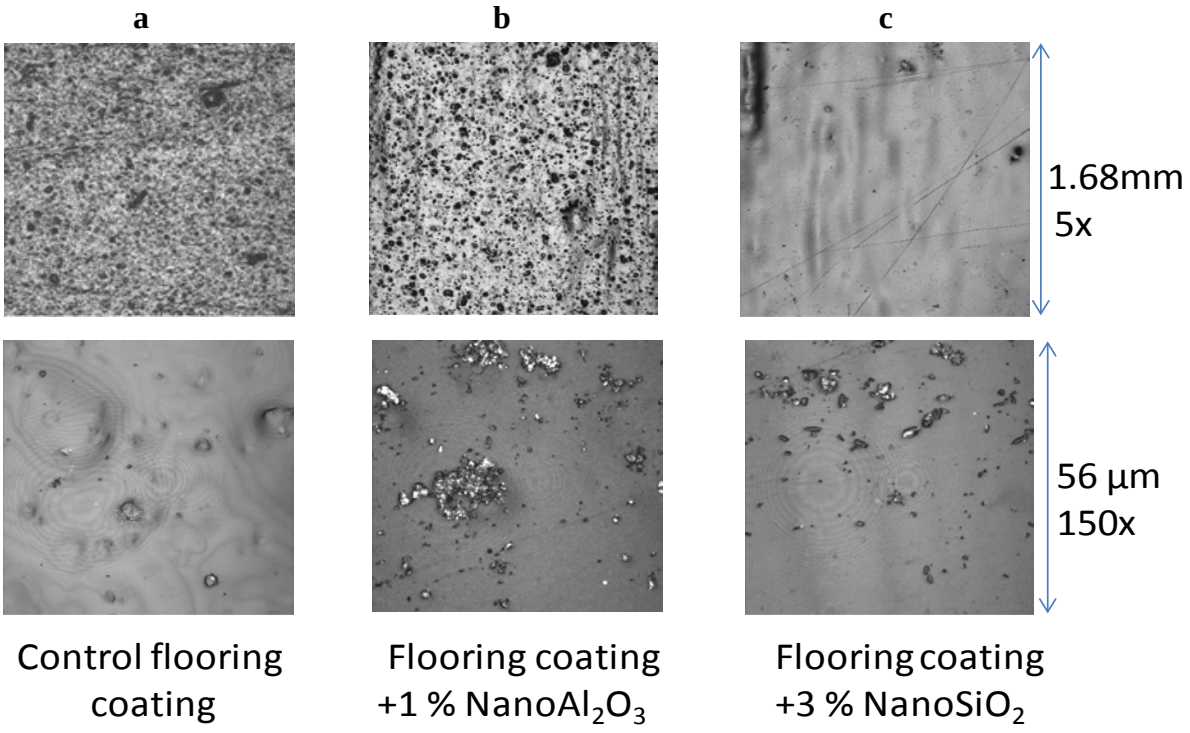

Figure 9a. LSCM images at 5x (upper row) and 150x (lower row) of unfilled and nano-filled PU flooring coatings on oak; a) unfilled PU, b) 1.0 % Al_2O_3 PU, and c) 3.0 % nanoSiO_2 PU.

LSCM images of the control and nano-filled latex paints at two magnifications are illustrated in Figure 9b. Again, the surface at low magnification exhibits a large variation in gray level, representing differences in surface roughness. On the other hand, the high magnification images show the presence of particles or clusters of nanoparticles. As described in the experimental section, the control latex paint is a commercial product containing 30 % nepheline syenite filler (aluminum silicate) that has a size ranging from 5 µm to 10 µm. Therefore, without chemical identification or other characterization techniques, it is not possible to distinguish these particles as due to the filler, clusters of nanoparticles, or residual cutting debris.

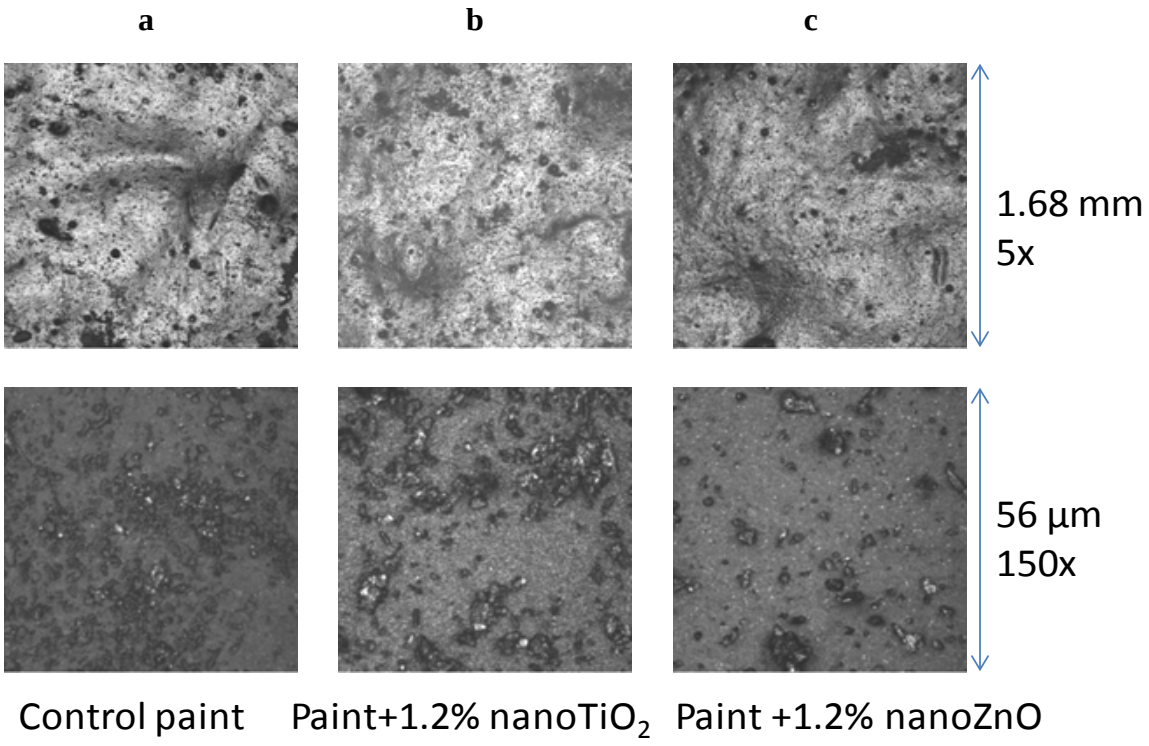

Figure 9b. LSCM images at 5x (upper row) and 150x (lower row) of control and nano-filled latex paints on drywall substrate; a) control, b) 1.2 % nanoTiO_2 paint, and c) 1.2 % nanoZnO paint.

The surface morphology of these nano-filled PU coatings and latex paints taken at a greater spatial resolution was characterized using the AFM technique, and representative images at different magnifications are shown in Figures 10a and 10b. The units given on the left are the scan size of each image. For each pair of micrographs, the topographic (height) image is on the left and the phase image is on the right. Large scan size (i.e., low magnification), such as 20 µm, provides useful information about the general features of a material surface while the small scan size can reveal details on the size and size distribution at the nanoscale spatial resolution of surface features. Phase images are included in this study because phase change of the AFM oscillating probe during scanning in the tapping mode is sensitive to material properties, such as modulus and chemical composition. Therefore, phase images often provide significantly more contrast than those obtained from topographic images. This is helpful for identifying of

nanoparticles that are covered by a thin layer of polymer or are beneath the surface in a polymer nanocomposite where the difference in topography is small.

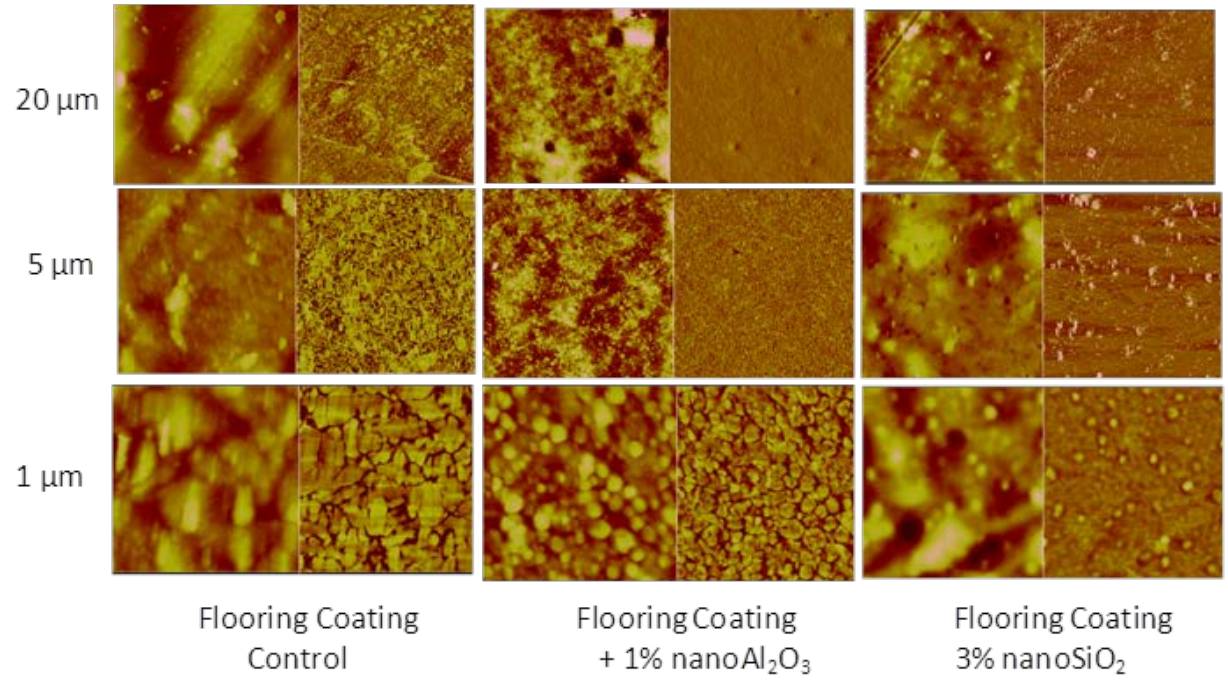

Figure 10a. Height and phase AFM images at different magnifications for unfilled and nano-filled PU flooring coatings. In each pair, height image is on the left and phase image is on the right.

The bright and dark areas in the height images correspond to the higher and lower topography, respectively, relative to the averaged plane of the imaged region. On the other hand, the bright domains in the phase image are generally attributed to the higher modulus regions than the surrounding darker regions. At a low magnification scan (20 µm scan), both height and phase images show the presence of particles. Finer surface features are observed at 5 µm scan size. At 1 µm scan size (also at 500 nm scan size, not shown), regular nanosize structures are clearly seen in both the unfilled and 1 % nanoAl_2O_3 PU coatings (bottom, far left and middle images). Comparing the images of these two coatings suggests that the regular nanostructure is the heterogeneous two-phase structure of the PU polymer, consistent with previous report (32). That is, the nanosize features in the nanoAl_2O_3 PU coating are not from the Al_2O_3 nanoparticles. On the other hand, the particles scattered on surface of the 3 % nanoSiO_2 PU coating (bottom, far right) are probably due to the nanoSiO_2 clusters. This interpretation is based on the low number,

the random distribution, the high nanoparticle loading, and the agglomeration characteristics of these particles.

AFM images of surfaces of the control and nano-filled latex paints are displayed in Figure 10b. The images of control paint at 5 µm and 20 µm scans show flake-like particles having sizes ranging from 0.5 µm to 5 µm, suggesting that they are probably aluminium silicate filler that was present in the paint. The nanosize, regular structure observed in the 1 µm scan of the control and nanoparticle-containing samples is probably due to the microstructure of the latex paint. The regular nanostructure can be more clearly seen in the 200 nm scan displayed in the inset of the nanoTiO_2 latex paint (bottom, far right). It should be noted that the presence of 30 % filler in the latex paint may alter the latex's microstructure. However, when properly dispersed, as for commercial products, each filler particle should be coated with a layer of the latex polymer. Therefore, the AFM technique, which images only the top 1 nm surface features, should show the structure of the latex film.

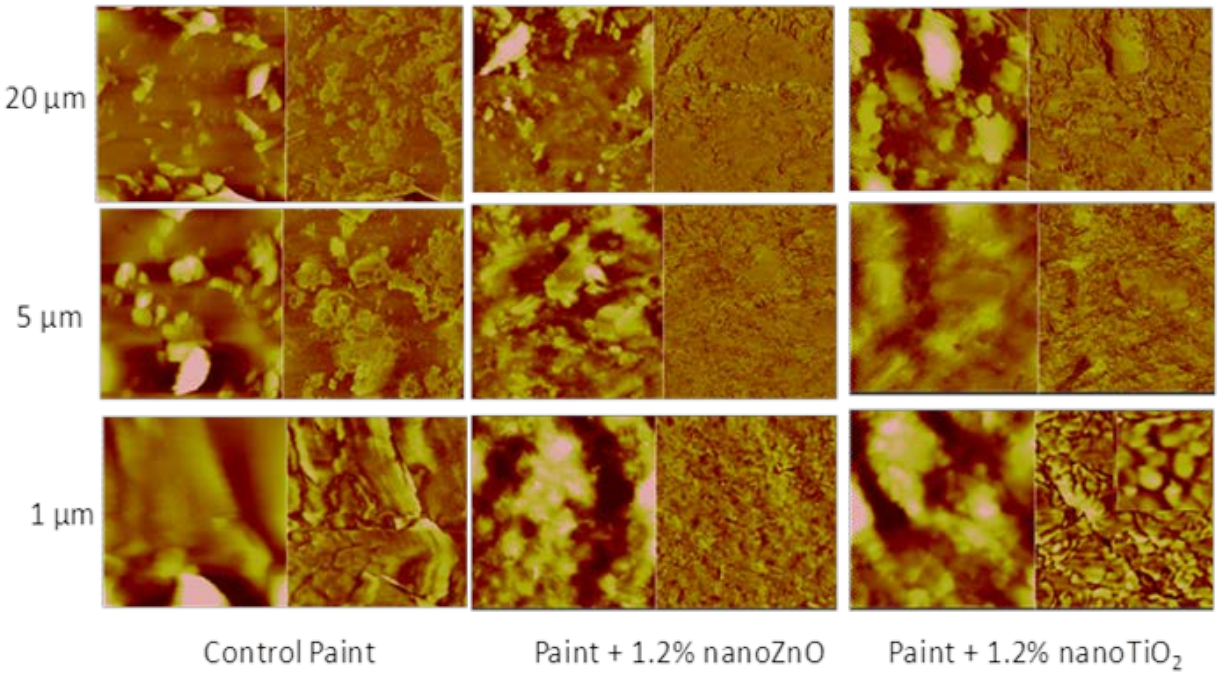

Figure 10b. Height and phase AFM images at different magnifications for control and nano-filled latex paints; the inset (bottom row, far right) is a typical 200 nm scan phase image of the 1.2 % TiO_2 paint, showing the latex microstructure. In each pair, the height image is on the left and phase image is on the right.

In summary, LSCM and AFM analyses show the presence of particles or clusters of nanoparticles on the surfaces of some nano-filled PU coatings and latex paints. Further studies are needed to determine whether these are from the nanoparticles incorporated in the matrices.

4.2 Surface Mechanical Properties of Nano-filled PU Flooring Coatings and Interior Latex Paints

Surface mechanical properties (modulus E and hardness H) of the control PU flooring coatings and latex interior paints and their nano-filled materials are presented in Table 3. The modulus of the control PU coating is similar to that of a polycarbonate material and that of the control latex paint is the same range to that of low density polyethylene. The presence of 1 % Al_2O_3 nanoparticles only slightly increases modulus of the PU coating, but incorporating 1.2 % TiO_2 nanoparticles into the latex paint improves its modulus by more than 40 %.

Table 3. Surface mechanical properties of PU flooring coating and latex paint with and without nanoparticles. The ± values represent one standard deviation from the averaged data of 15 indents.

Materials	**E (GPa)**	**H(GPa)**
Control PU coating on wood	2.40 ± 0.29	0.11 ± 0.01
PU + 1% nanoAl_2O_3 on wood	2.46 ± 0.14	0.12 ± 0.01
Control latex paint on drywall*	0.23 ± 0.14	0.005 ± 0.002
Control latex paint + 1.2 % nanoTiO_2*	0.33 ± 0.06	0.04 ± 0.002

*The hardness values of the latex paint are believed to be incorrect because nanoindentation technique does not reliably measure the hardness of soft materials.

4.3. Feasibility of LSCM for Quantifying Distribution of Abrasion-induced Release Particles Accumulated on Coated and Painted Surfaces

Figure 11 shows several panels, as an example, of 1 % nanoAl_2O_3 PU coating that had been abraded with the Taber abraser at two different wheel speeds and two different numbers of cycles. The abrasion used a fixed load of 1000 g and a CS-10 wheel under vacuum. The circular abraded areas in Figure 11 are clearly visible with the naked eye, indicating that the top layer of these surfaces has been removed by the abrasion process, consistent with an increase in roughness following abrasion.

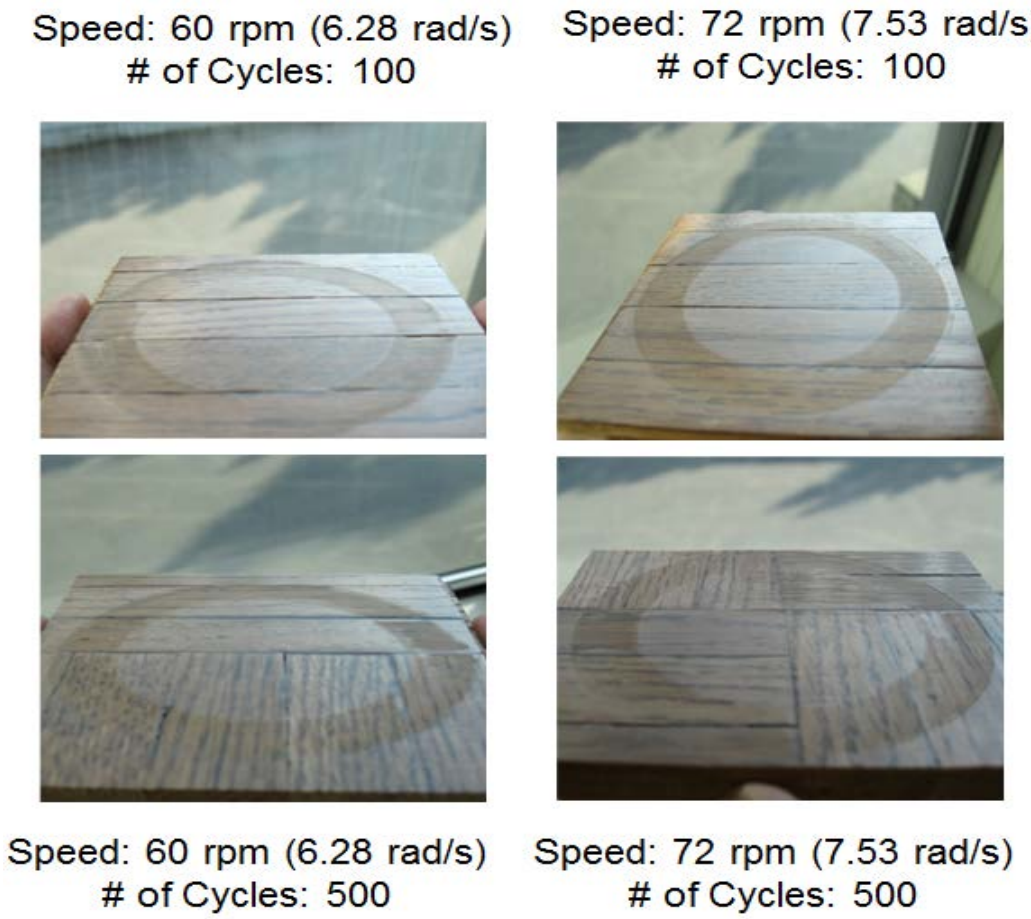

Figure 11. Pictures of several abraded nanoAl_2O_3–filled PU coated oak panels for different abrasion parameters, showing the loss of surface gloss in the abrasion area.

As stated in the experimental section, 16 LSCM images were taken from each abraded panel. For the nanoAl_2O_3 PU coating, three number of cycles and two wheel speeds were employed. In addition, a specimen of the unfilled PU coating was abraded at a fixed number of cycles and one speed. Thus, a total of 112 LSCM images were taken for assessing the suitability of LSCM for quantifying abrasion surface release particles. Figure 12 displays four representative LSCM images, which were taken from the center position (Position # 2 in Figure 8), from four different panels. As indicated above, the bright regions in a LSCM image are due the greater reflection from the objects that are above the surface, and the darker regions represent the objects that are below the surface. Thus, the bright particles observed in these images are believed to be the particles generated by the abrasion. The abrasion marks can be clearly seen in these LSCM images.

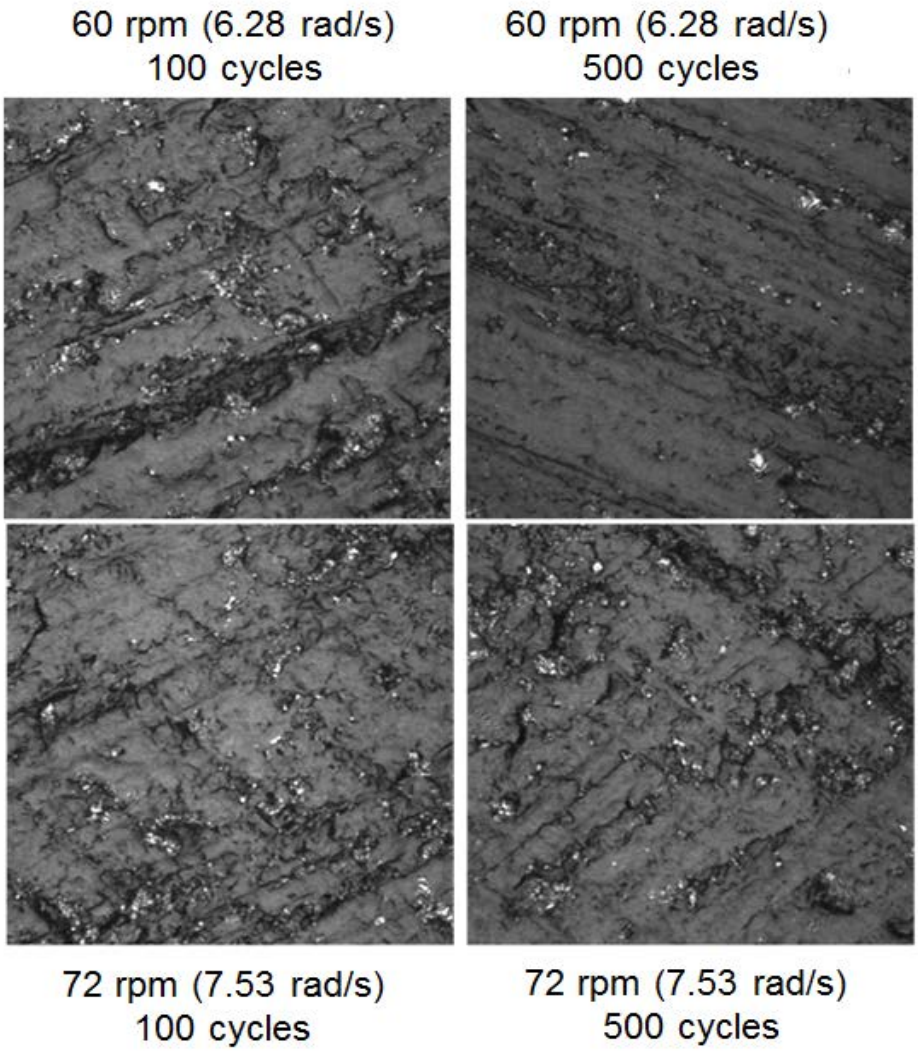

Figure 12. Representative 150x LSCM images of abraded nanoAl_2O_3 PU flooring coating for two abrasion speeds and at two numbers of cycles. The image size is 56 μm x 56 μm

Applying the *ImageJ* software program and carefully adjusting the gray level, the total number and size distribution of particles in the 56 μm x 56 μm abraded area from each 150x LSCM image can be obtained. An example is displayed in Figure 13. In this figure, 13a is a 150x LSCM image of the abraded surface, 13b is the gray level threshold setting, 13c is the highlighted particles within the image as defined by the gray level threshold, 13d is the black and white image corresponding to the highlighted particles, 13e is the particle counting figure which tallies the number of particles for each particle size, and 13f is the bar plot of the total particles for each size from 0.1 μm to 0.6 μm. A visual comparison between Figures 13a and 13d would validate the gray level threshold selection.

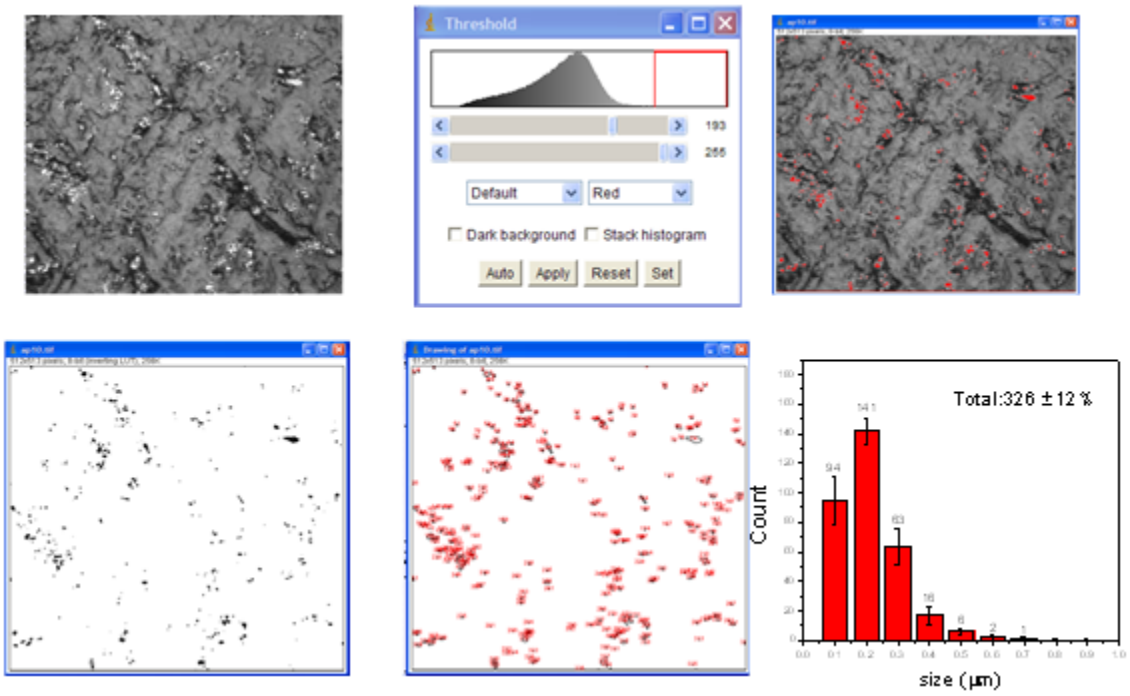

Figure 13. An example of analysis of LSCM images for abraded nano-filled PU flooring coating surfaces to obtain the total number and size distribution of surface release particles generated by abrasion. The abrasion parameters are speed 72 rpm (7.53 rad/s), loading 1000 g, and 500 cycles. Error bars represent one standard deviation.

Table 4 gives a summary of the number and size distributions of particles present in a 56 µm x 56 µm (3.136×10^{-3} mm^2) area on the nanoAl_2O_3 PU coating surface after being abraded at two speeds, three numbers of cycles, and one fixed loading. The results for the control PU specimen abraded at one speed and a set number of cycles are also included in Table 4 for comparison. All results are the average of 16 LSCM images on the circular abraded area of a specimen. The total number of particles and their size distributions per unit abraded area for each material specimen can then be obtained. The % value at the bottom of each column is the coefficient of variation (100 x standard deviation/means). Except for the results of two columns which have a coefficient of variation larger than 25 %, the reproducibility of other results are below 20 %, which is considered to be acceptable. Undoubtedly, the surface roughness, the gray level threshold selection, and the variability of particle distribution during the abrasion probably

contribute to the high standard deviation values. It should be noted that surface release particles tend to accumulate on the outside of the circular abraded ring. The results show that for the same abrasion parameter, nanoAl_2O_3–filled PU coating generated more surface release particles than the unfilled PU. At 72 rpm (7.53 rad/s) speed, the number cycle has a minimum effect on the surface release particles for all sizes. However, the number of cycles appears to have a noticeable effect at 60 rpm (6.28 rad/s), with the highest number of cycles yielding the smallest number of particles, both for the total number and for each size from 0.1 µm to 0.4 µm. The majority of surface release particles on abraded nanoAl_2O_3 PU coating have a size ranging from 0.1 µm to 0.4 µm, with the 0.2 µm size having the greatest number of particles. These size results are in agreement with previous studies on airborne particles emitted by the Taber abraser for polymeric coatings containing nanoZnO (26), nanoTiO_2 (27), and MWCNT epoxy composites (21), which reported particle sizes ranging from 0.1 µm to < 50 µm.

Table 4. The number of particles for each size in a 56 µm x 56 µm abraded area on unfilled and nanoAl_2O_3-filled PU flooring coatings abraded at two speeds, three number of cycles, and a fixed 1000 g applied load. The % value at the bottom of each column is the coefficient of variation (100 x standard deviation/means). Note that 72 rpm= 7.53 rad/s and 60 rpm= 6.28 rad/s.

Parameters: Speed (rpm) Loading (g) # of Cycles Particles size (um)	72 1000 100	72 1000 200	72 1000 500	60 1000 100	60 1000 200	60 1000 500	72 1000 200 Control
0.1	76	85	76	86	67	41	31
0.2	130	153	135	149	124	71	49
0.3	51	61	61	61	59	33	20
0.4	23	23	23	21	17	10	4
0.5	14	7	7	7	6	3	2
0.6	5	3	2	2	2	1	1
0.7	2	1	1	1	1	2	0
Total	280 ±14%	337 ±18%	309 ±29%	331 ±14%	279 ±18%	160 ±15%	109 ±34%

One should be careful about interpreting the results on the effect of abrasion cycles on the number of particles accumulated on the specimen surface using a Taber abraser. The reason is the wheel rotation on the specimen at a particular cycle might move, redistribute, or add to the number and distribution of surface release particles that were produced by the previous abrasion cycle or cycles. This should not be a problem for airborne release particles, but likely complicates the effect of cycle on the number and distribution of surface release particles. This is likely one main reason for some high standard deviation values shown in Table 4. Further research is being carried out to address this issue.

To confirm that the bright particles observed in Figure 12 are mainly due to the particles generated by the abrasion process, a procedure using an adhesive tape was used. For this purpose, a transparent pressure sensitive adhesive tape was applied on the abraded surface and rolled forward repeatedly for 10 times with a tweezers at an applied normal load of approximately of 255 g ± 5 g, which was measured with a hand held balance. The adhesive tape was immediately removed, and both the abraded and adhesive tape surfaces were imaged and analyzed by LSCM at 150x magnification. One example of the results for the nanoAl_2O_3 PU coating is displayed in Figure 14. Before applying the adhesive tape, a total of 301 particles were recorded in the abraded 56 μm x 56 μm surface, and only a few particles were seen on the adhesive tape surface (Figure 14, upper row). After applying the adhesive tape, the number of particles on the abraded surface decreased substantially, and numerous particles and their clusters are seen on the tape surface (Figure 14, upper row). Similar results were observed for the control PU coating (not shown), though the number of particles are fewer, as reported in Table 4. These results suggest that a substantial number of particles on the abraded surface are loosely attached particles and can be removed readily by an adhesive tape. The remaining particles on the abraded surface after the tape application are probably those lying in the valleys of the surface and were not in contact with the applied tape.

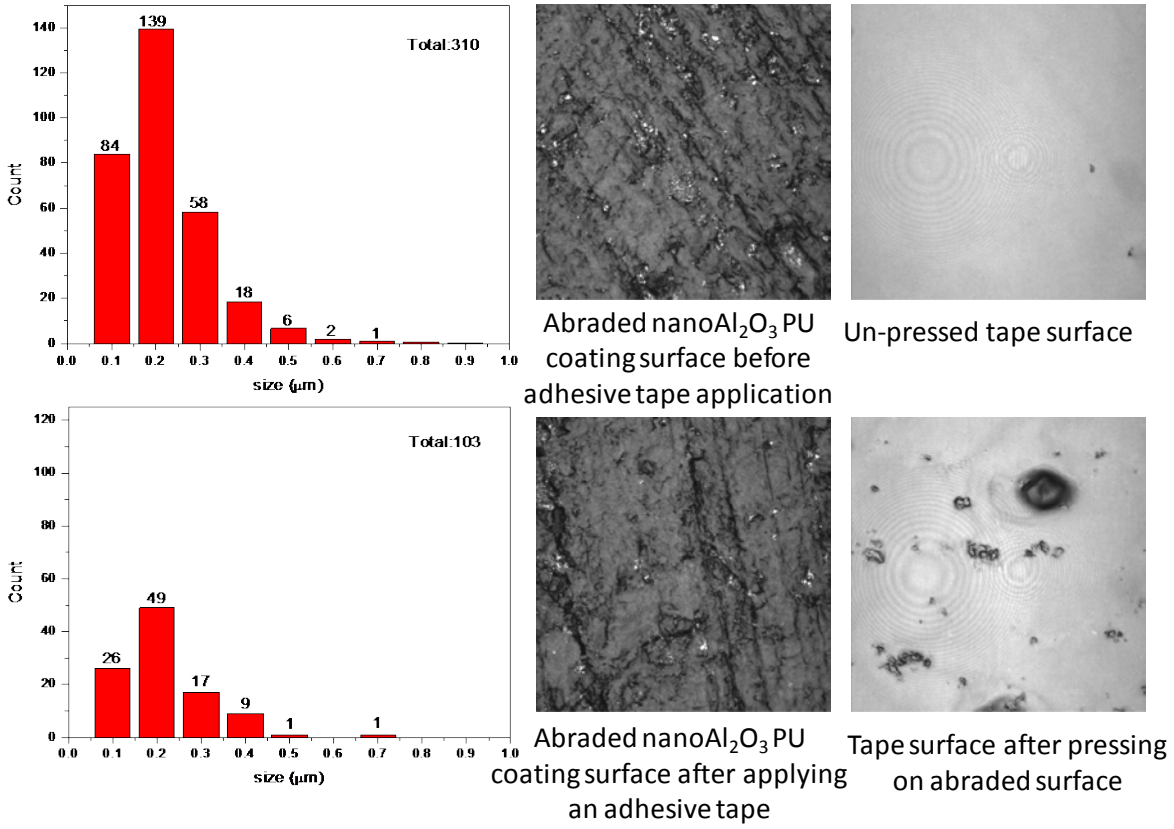

Figure 14. Effects of adhesive tape application on the number of particles and appearance of abraded nanoAl_2O_3 PU coating surface. Upper row: particle counts, LSCM images of abraded coating, and adhesive tape surfaces before the tape application; lower row: particle counts, LSCM images of abraded coating, and tape surfaces after the tape application. The image size is 56 μm x 56 μm, and the uncertainty for the particle count is <15 %.

4.4. Effects of Abrasion Parameters and Wheel Type on Release Particles Accumulated on the Nano-filled Coating and Paint Surfaces

4.4.1. Effects of Wheel

The mechanical properties and composition of the abrading wheel play an important role in the number and size distribution of particles generated by abrasion of polymer nanocomposites. Only two studies have reported the use of different type of wheels for abrasion. Ref. (26) reported three types of wheels, CS-10, CS-17, and H-18 (composition: rubber + alumina + silica) were employed in their study of airborne particles generated by abrasion for several polymers containing ZnO nanoparticles. However, they did not present the results for each type of wheel or discuss the effect of wheel type. On the other hand, Ref. (27) found that

the S42 wheel (aluminium oxide grit sand paper) released more particles into the air, mostly microscopic size, than the CS-17 wheel. This study also observed that the S42 wheel generates 500 times more particles when abrading on a glass substrate surface than on a paint containing TiO_2 nanoparticles. No explanation was given. When using wheels containing polymer matrix and inorganic particles, like the CS-10, CS-17 or H-18, the soft matrix material would likely wear out and the wheels themselves may generate the particles. For normal testing of the wear or abrasion resistance of polymer coatings, as specified by the ASTM standards, this is not a problem because any generated particles that lie on the abraded surface are blown off or cleaned before weighing the residual mass of the sample. However, for studies of airborne or surface release particles by mechanical forces, the particles generated from the abrading wheel will complicate the interpretation of the results. To address this question and to provide data for selecting a suitable wheel type for the surface release particles as well for airborne particles, we have investigated both polymer matrix (CS-10 and CS-17) and wear resistant tungsten carbide (S-35) wheel. The abrasiveness of these wheels imposed on a substrate surface is indicated in Table 2.

Figures 15 and 16 show the abraded surface characteristics and number and size distribution of particles generated on the surfaces of nanoAl_2O_3 PU coating and nanoTiO_2 paint, respectively, by the CS-10, CS-17 and S-35 wheels. The abrasion parameters used for these specimens are given in the bar plots. Further, no vacuum was employed for this set of results. Because of the severe impact and heavy mass of the S-35 wheel, the abrasion parameters used for this wheel were also different. For the nanoAl_2O_3 PU coating, little difference in the surface appearance is evident, as observed by the naked eye or by LSCM at 150x, and the number or size distribution of particles between the CS-10 and the CS-17 wheel. Similar results are observed for the control PU or nanoSiO_2 PU coating (not shown). However, for the nanoTiO_2 latex paint, a substantial amount of large green particles is observed on the surfaces abraded with CS-10 and CS-17 wheels, with a greater amount for the latter wheel type (far left images, top and middle rows). Because green is the colour of these two wheels, the results suggest that these large green particles are due to the wearing of the wheels themselves. The results of Figure 16 also suggest that the CS-17, which is recommended for testing of more wear resistant materials, wore down more rapidly and generated many more particles than the CS-10 wheel. Similar surface characteristics were observed for abraded control latex paint surfaces, as shown in the insets. Chemical analyses are being carried out to determine whether these green particles contain any

alumina abrasive particles. The difference in the release of wheel materials between the PU and the latex paint may be due the differences in mechanical properties between the two materials. As seen in Table 3, the modulus (stiffness) of the nanoAl_2O_3 PU coating is about 10 times greater than that of the nanoTiO_2 latex paint. Further study is needed to confirm this explanation. If the green particles observed on the specimen surfaces indeed include the material generated by the CS-10 and CS-17 wheels themselves, they may also be included in the total of particles detected in the air. However, References 26 and 27 used the rubber-abrasive wheels but did not report or discuss the effect of wheel material on the total airborne particles measured by SMPS or other techniques. On the other hand, Ref. (21) reported the number of particles released from the H-18 wheel is small and does not contribute to the total number of airborne release particles.

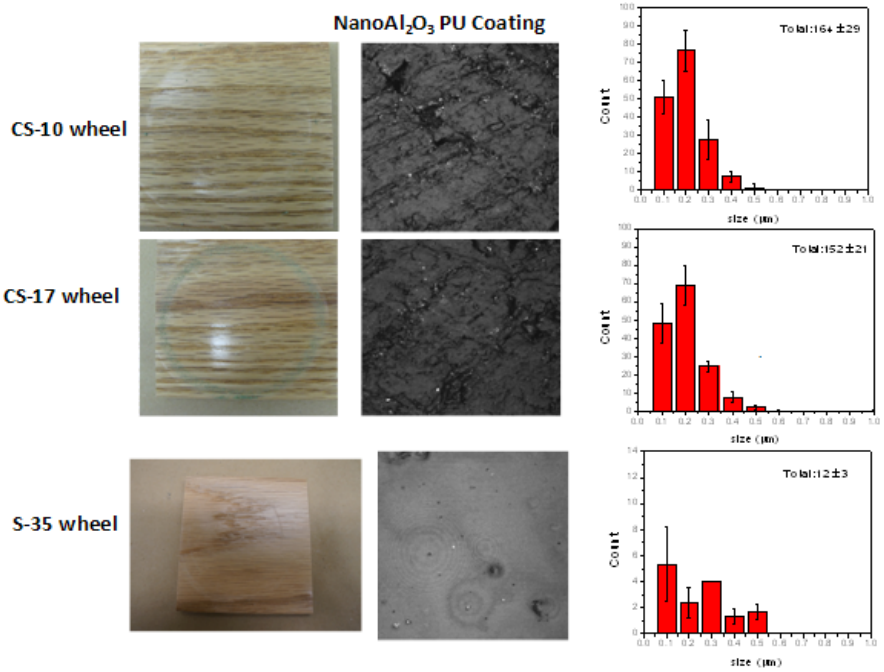

Figure 15. Effects of wheel type on the abraded surface characteristics and number of surface release particles for nanoAl_2O_3 PU coating. The abrasion parameters are speed 60 rpm (6.28 rad/s), loading 1000 g, and 100 cycles. For each wheel type, a picture of the abraded surface is on the left, the LSCM image at 150x is in the middle, and the number and size distribution of surface release particles is on the right. Abrasion parameters are given in the bar plots. Error bars represent one standard deviation.

As seen in these figures, although the S-35 (tungsten carbide) generated fewer surface release particles, the absence of the green material on the abraded surfaces suggests that this wheel was

probably not worn out by the abrasion process and, therefore, should not interfere with the total number or size distribution of surface release particles. This result is encouraging because, for study of abrasion-induced release particles both in the air or accumulated on the specimen surface using a Taber abraser, the particles generated from the wheel itself must be accounted for, which would be difficult for repeated cycles.

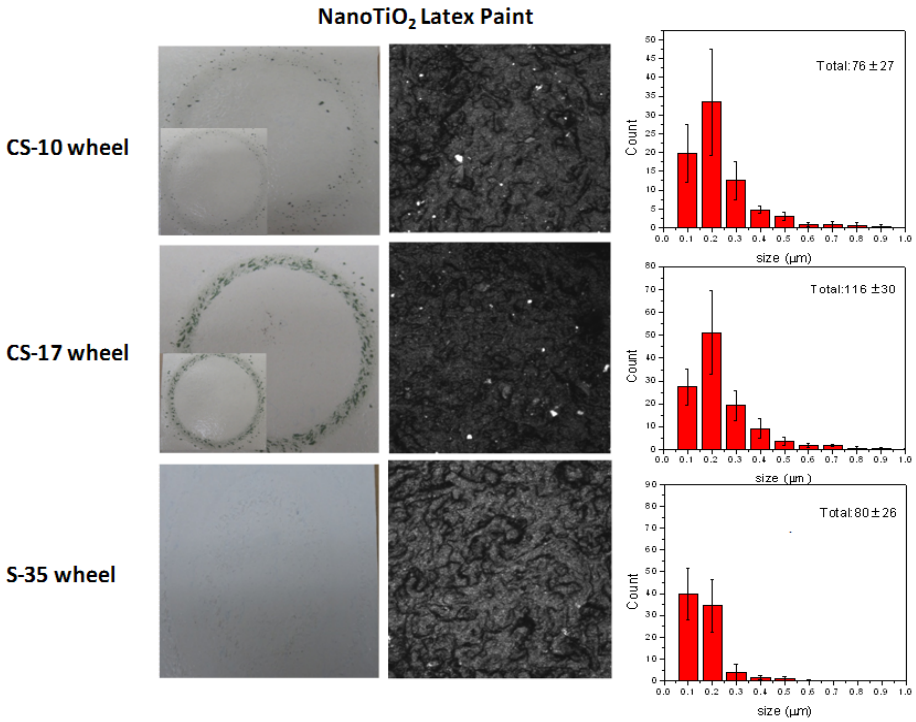

Figure 16. Effects of wheel type on the abraded surface characteristics and number of surface release particles for nanoTiO_2 latex paint. The abrasion parameters are speed 60 rpm (6.28 rad/s), loading 1000 g, and 100 cycles. For each wheel type, a picture of the abraded surface is on the left, the LSCM image at 150x is in the middle, and the number and size distribution of surface release particles is on the right. The insets in the pictures (far left on top and middle rows) are from control latex paint, showing a greater amount of green particles by the SC-17 wheel than the CS-10 wheel. Error bars represent one standard of deviation

It should be noted that these results and others (not shown) obtained for other nano-filled PU coatings and latex paints showed that the standard deviation for the number of surface release particles generated by the S-35 wheel is, in general, much greater than those for the CS-10 or CS-17 wheel. This is likely due to the fact that the S-35 wheel consists of large and sharp grooves, which tend to hold the particles and produce very rough and uneven surfaces. This

greatly affects the accumulation and distribution of surface release particles. Because of the encouraging result offered by the S-35 wheel, NIST is investigating the use of metallic wheels that have fine textures similar to those of the matrix-abrasive wheels to produce relatively smooth surface for generating surface release particles. The results of that investigation will be included in the second year report.

4.4.2. Effects of Vacuum

As indicated in the experimental section, the Taber abraser is equipped with a vacuum nozzle that can be used to remove generated particles. The effect of the vacuum on the number and size distribution of abrasion-induced surface release particles was evaluated for nano-filled PU coatings and latex paints. When operating with a vacuum, the vacuum nozzle was set at 4 mm above the specimen surface. The results are summarized in Figure 17 for nanoAl_2O_3 PU and nanoTiO_2 paint using the CS-17 wheel.

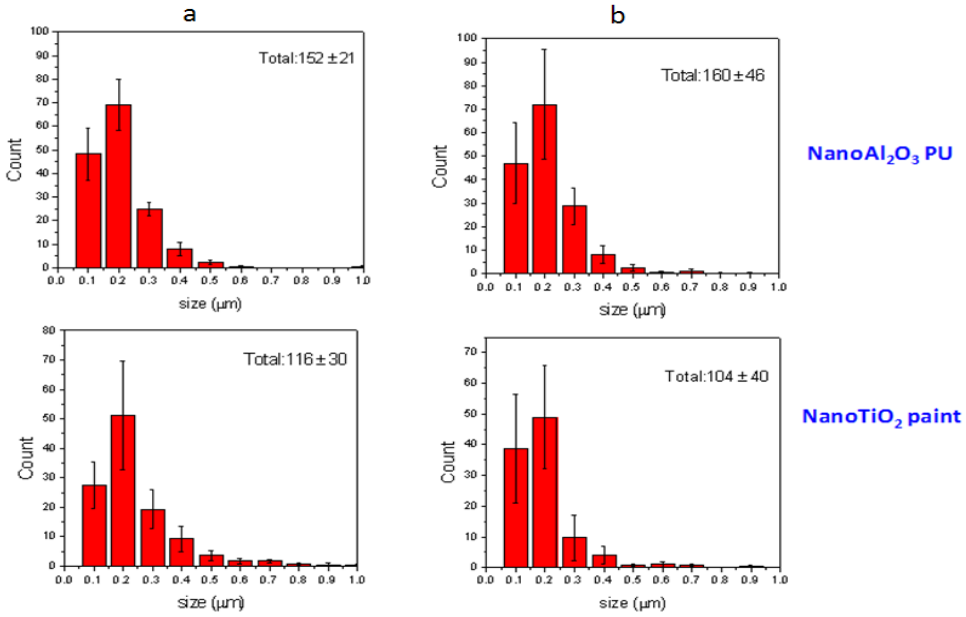

Figure 17. Effect of vacuum on the number and size distribution of surface release particles; a) with a vacuum, and b) no vacuum. A CS-17 wheel was used, and the abrasion parameters are speed 60 rpm (6.28 rad/s), loading 1000 g, and 100 cycles. Error bars represent one standard deviation.

The vacuum appears to have little effect on both the total and size distribution of surface release particles, suggesting that the released particles stick rather strongly to the abraded surfaces.

4.4.3. Effect of Abrasion Cycle and Applied Load

Figure 18 shows the effects of abrasion applied load and number of cycles on the number and size distribution of surface release particles for, as examples, nanoAl_2O_3 PU flooring coating and nanoTiO_2 interior latex paint. At high applied load (1000 g), the abrasion cycle appeared to influence the number and size distribution of the stiff nanoAl_2O_3 PU coating; that is, the number of particles appeared to decrease with increasing number of cycles. For this material, the higher load also appeared to generate more particles than the lower load. The difference is more noticeable at 300 cycles or lower. However, both the number of cycles and the applied loading did not seem to have an effect on the number or size distribution of soft nanoTiO_2 latex paint. As previously pointed out, the result of the abrasion cycle effect on the number of surface release particles needs to be considered with caution because of the repeated rotary action of the wheel on the specimen.

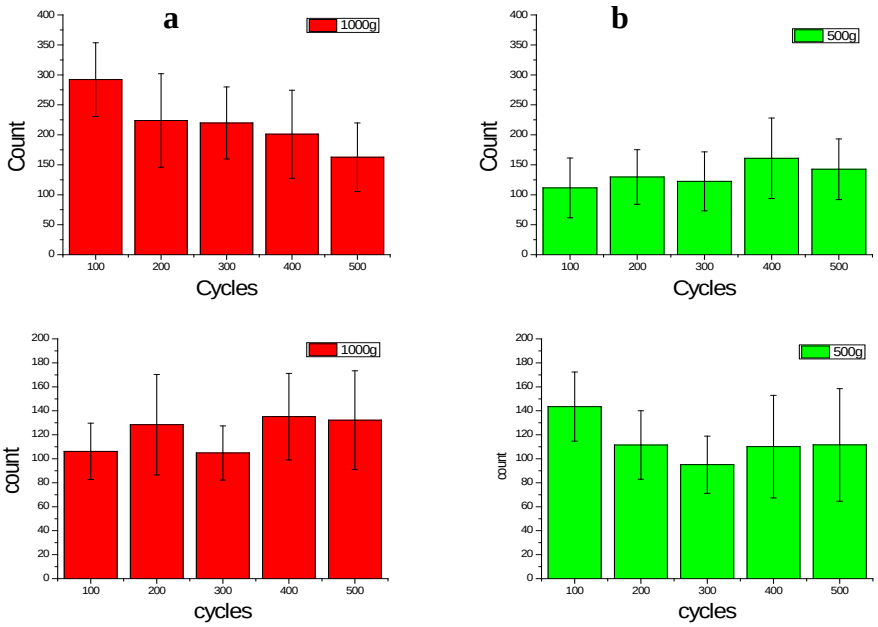

Figure 18. Effects of abrasion cycle and applied load on the number and size distribution of surface release particles for nanoAl_2O_3 PU coating (upper row), and nanoTiO_2 latex paint (lower row): a) 1000 g loading, and b) 500 g loading. A CS-10 wheel was used. Error bars represent one standard deviation.

4.5 Characterization of Abraded Surfaces and Surface Release Particles

4.5.1. Characterization of Surface Release Particles

Released particles accumulated on the surface of nano-filled PU coatings and latex paints by abrasion were characterized by ICP-MS and SEM techniques, and surfaces of the abraded specimens were investigated by LSCM, XPS, SEM, and AFM. (TEM analysis of surface release particles, which was contained in the proposal, will be included in the study of airborne particles generated by the same abrasion process.)

Figures 19 and 20 present SEM images of particles generated by the abrasion of nano-filled PU coatings and nano-filled latex paints, respectively, using a S-35 wheel. As indicated in the experimental section, the particles were collected on TEM Cu grids by pressing the grids against the specimen surface after abrading at a particular set of parameters. Both secondary electron (SE) and backscattering electron (BSE) images were obtained to provide geometry and characteristics of the surface release particles. SE mode provides a better spatial resolution while BSE mode can give useful information about chemical composition of the material.

Figure 19a displays SEM images of typical particles generated by the S-35 wheel on the surface of the PU flooring coating containing 3 % 30 nm diameter SiO_2 nanoparticles. The 500 μm scan SE image (Figure 19a, upper row, far left) exhibits an example of the particles collected on a Cu grid. At least two types of particles were observed when an S-35 wheel was employed to abrade this nano coating, as observed in the SE images at 5 μm scan size (Figure 19a, upper row, middle and far right). Type 1 particles appear shredded and torn off (upper row, middle), probably resulting from the tearing action of the abraser. High magnification BSE of this particle type (lower row, far left) shows no evidence of nanoscale materials present on the surface of this type of particle. Type 2 particles (upper row, far right) appear as ruptured, probably resulting from fracture of the nanocomposite coating. High BSE images (lower row, middle and far right) show the presence of nearly round particles having diameters ranging from 20 nm to 60 nm on the particle surface. These particles are probably individual particles, or clusters of a few SiO_2 nanoparticles that were incorporated in the PU coating. Chemical analysis is being carried out to confirm this postulation.

Abrasion with an S-35 wheel also appeared to generate at least two types of particles from the nanoAl_2O_3 PU coating, as observed in the SE images displayed in Figure 19b (upper row). One type has a ruptured appearance (upper row, middle) while the other type appears as flakes. High magnification BSE images (middle and bottom rows) show the presence of

nanosize particles (bright spots). Again, chemical measurement is being made to determine whether these nanosize features are from the 20 nm diameter Al_2O_3 particles that were incorporated in the PU coating.

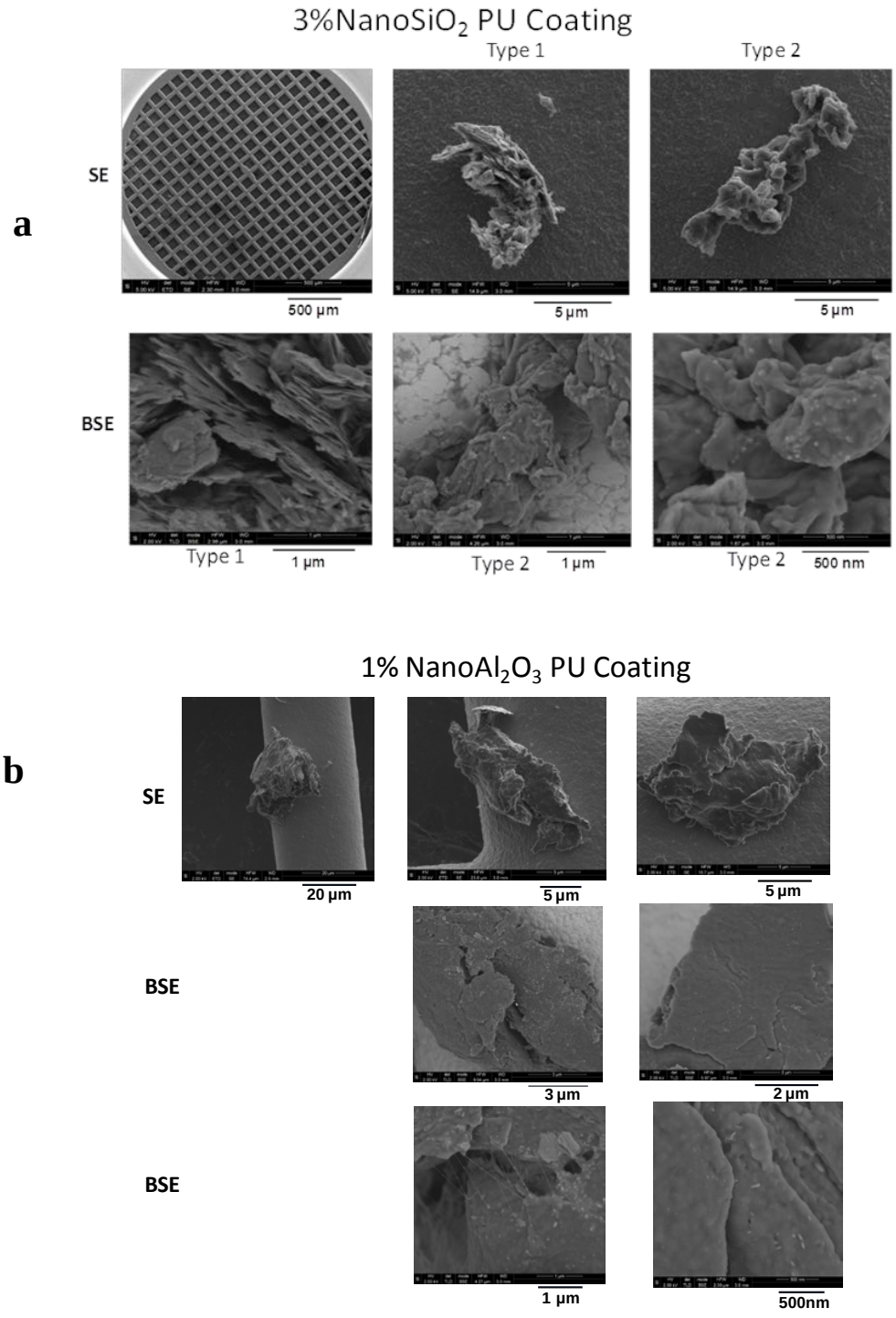

Figure 19. SEM images of surface release particles generated by the S-35 wheel for nano-filled PU flooring coatings, a) 3 % nanoSiO_2 PU, and b) 1 % nanoAl_2O_3.

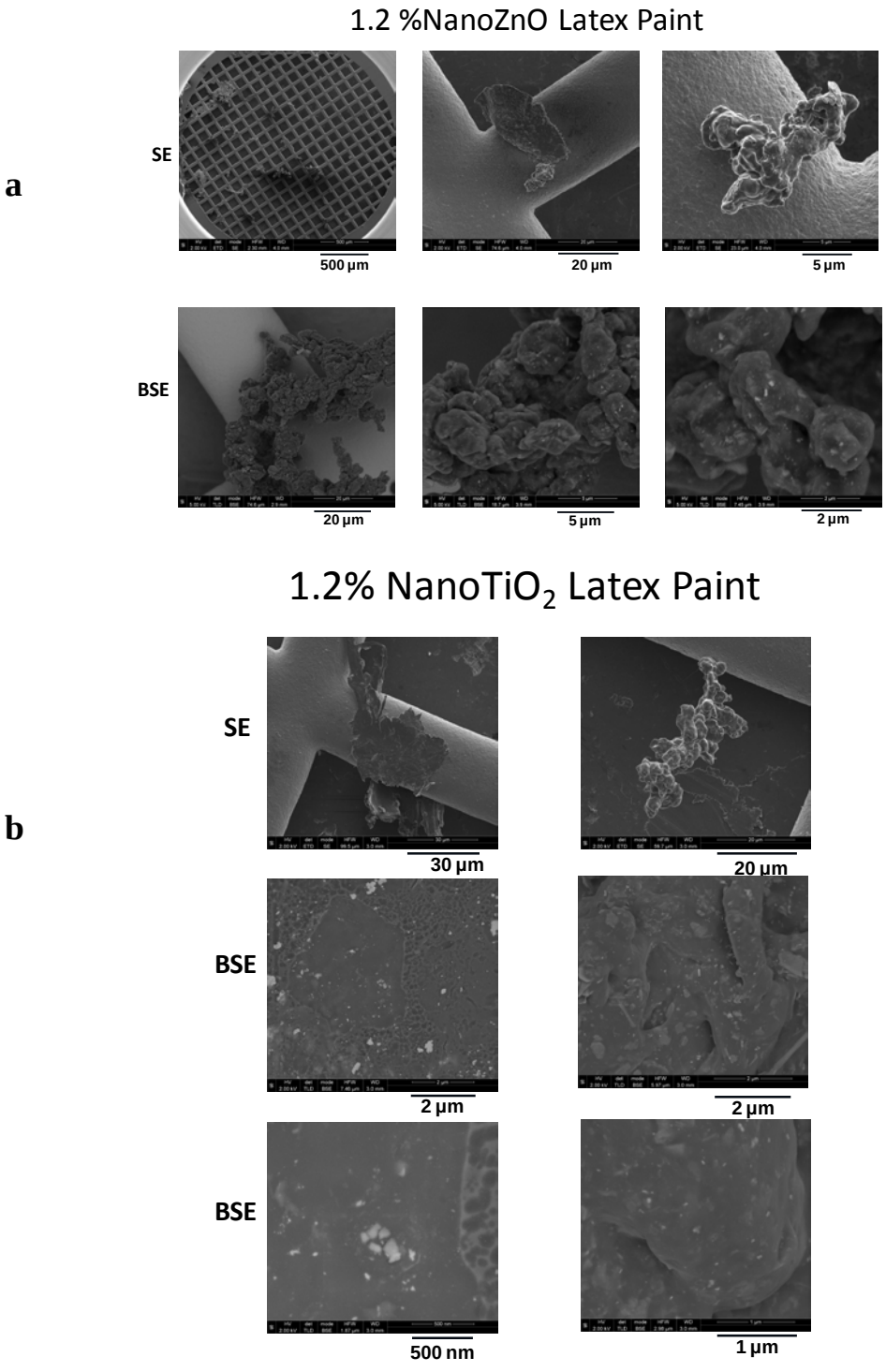

Figure 20. SEM images of surface release particles generated by the S-35 wheel for nano-filled latex paint, a) 1.2% nanoZnO paint, and b) 1.2 % nanoTiO_2 paint.

SEM images of surface release particles from nano-filled latex paints abraded with an S-35 wheel are displayed in Figure 20. SE images (Figure 20a, upper row) of the nanoZnO paint at different magnifications show the particles collected on a Cu TEM grid and surface morphology of the particles, showing a ruptured appearance and irregular shape. BSE images at high magnifications (Figure 20a, lower row, middle and far right) show the presence of nanosize features (bright spots) on the particle surfaces. SE and BSE images of surface release particles from nanoTiO_2 latex paint show both flake-like and ruptured appearances (Figure 20b). High resolution images reveal the presence of numerous nanosize features (bright spots) having round and non-round shapes. The nanosize bright spots in Figures 20a and 20b are probably from the ZnO and TiO_2 nanoparticles, respectively. This postulation is consistent with the XPS data, which detected Ti and Zn on the corresponding abraded surfaces (see Table 6). Further chemical analyses are being carried out to substantiate this evaluation.

Figures 19 and 20 clearly show that the surface release particles generated by abrasion with the S-35 wheel contain nanosize features. Further analyses are being carried out to determine the chemical composition of these nanosize features. If they are indeed from the nanoparticles that were incorporated in the flooring coatings and paints, their presence on the release particle surfaces may have a health and safety implication.

A qualitative ICP-MS analysis was carried out to determine whether individual nanoparticles are present in surface release particles generated from nano-filled PU coatings and latex paints. As indicated in the experimental section, the surface release particles were placed in bottles containing 25 ml de-ionized water, and only the supernatant in each bottle was analyzed. Thus, only elements dissolved, or nanoparticles suspended, in water were detected. The results are presented in Table 5 for the eight types of surface release particles generated by abrasion using two wheel type on six materials. CS-10 wood, CS-10 drywall, and S-35 drywall refers to the control PU coating on wood and control paint on drywall abraded with CS-10 and S-35 wheels. It should be noted that the CS-10 wheel, which is composed of rubber and alumina abrasives, was observed to release its own particles during the abrasion, as presented earlier. While the S-35, which is made up of tungsten carbide, is not expected to release any material. Table 5 shows that, except for a small amount of Zn element (14 ng/g metal), there is little evidence of any element dissolved or suspended in the solution for the surface release particles generated by the S-35 wheel from both control paint and nanoTiO_2 paint. Further, there is also no evidence of any element from the particles generated from the nanoSiO_2 PU coating abraded

with a CS-10 wheel. The absence of Al in this (liquid) sample suggests that the materials released by the CS-10 wheel do not contain nanosize aluminium oxides nor do the aluminium oxides from the wheel do not dissolve in water. The presence of a very small amount of Ti in the nanoTiO_2 paint sample also suggests that a small amount nanoTiO_2 was not dissolved or suspended in water. On the other hand, a substantial amount of Zn (110 ng) found in the latex paint containing nanoZnO sample suggests that some ZnO in the surface release particles were dissolved or some ZnO nanoparticles were suspended in water. The presence of a large amount of Al and Si in the control and nano-filled latex paints abraded by the CS-10 wheel is consistent with the fact that the latex paint contained 30 % aluminium silicate. Obviously, some of this filler was dissolved by water. Further quantitative, systematic study will be carried out to determine the concentration of each element present in both the supernatant and the precipitates.

Table 5. ICP-MS results for surface release particles released from control and nano-filled flooring coatings and latex paints

in ng/g unit*	**Al**	**Si**	**Ti**	**Zn**	**W**
CS10 Wood	3.0	15.3	<0.1	12.0	0.02
CS10 drywall	70.9	130.3	1.9	1.5	<0.01
CS10 TiO_2	25.9	60.3	1.5	0.7	<0.01
CS10 ZnO	12.9	12.3	0.1	110.0	0.02
CS10 SiO2	0.7	<1	<0.1	1.3	<0.01
S35 drywall	0.6	3.1	<0.1	2.9	0.07
S35 TiO2	0.5	3.4	<0.1	2.8	0.05
S35 Al2O3	0.7	1.5	<0.1	14.0	<0.01
LOD	*0.1*	*1.1*	*0.1*	*0.02*	*0.01*

*Results are ng/g metal in 25 g solution.

Expanded uncertainty is 50 % of the measured value.

4.5.2. Characterization of Abraded Surfaces

Abraded surfaces are characterized by LSCM, SEM, AFM, and XPS. The LSCM results, which were measured on 100 mm x 100 mm panels, have been shown in Figures 9, 12, and 13. SEM, AFM, and XPS are analysed using the 10 mm diameter discs that were abraded with the S-35 wheel. SEM and AFM analyses are not completed and will be reported in the second year report. This section presents preliminary XPS results.

Table 6 presents the concentrations of elements present on the abraded specimens of control paint (ctrl), nanoZnO paint (ZnO), and nanoTiO_2 paint (TiO). C element is from the polymer and O comes from both polymer and oxides. In addition to Si and Al from the aluminium silicate, this control latex paint is also found to include compounds containing S, Na, F, and Ca. Although the concentrations of Ti and Zn are low, which is expected for a low nanoparticle loading (1.2 %), the results suggest that these elements are present on the abraded surfaces of nanoTiO_2 and nanoZnO latex paints, respectively. These results were measured from only one specimen to evaluate the technique, and thus no uncertainty can be given. Replicates will used to confirm these results and will be compared with elemental analysis by the SEM technique.

Table 6. Elemental concentrations for abraded surfaces of control paint and nano-filled latex paints

Name	Al %	C %	Ca %	F %	Na %	O %	S %	Si %	Ti %	Zn %
ZnO	0.3	62.8	2.1	1.1	1.7	27.2	3.6	1.1	0.0	0.1
TiO	0.3	65.8	1.6	1.9	0.8	25.7	2.2	1.6	0.1	0.0
Ctrl	0.5	67.7	1.1	2.2	1.0	24.3	1.6	1.6	0.0	0.0

5. Summary of Preliminary Findings and Further Studies

Polyurethane flooring coatings and interior latex paints with and without several nanoparticles have been abraded with a Taber rotary abraser to develop testing and measurement protocols for determining the quantities and properties of released nanoparticles in the air and accumulated on surfaces of flooring finishes and interior paints. In the first year of this research, we have examined the effects of abrading parameters and abrasive wheel type on the number and size distribution of release particles accumulated on the surfaces. In the first year, we have also investigated the suitability of laser scanning confocal microscopy (LSCM) as a technique for reliably quantifying the number and size distribution of release particles on abraded surfaces. A number of analytical techniques were employed to characterize surface morphology of nanocomposite coated and painted substrates, abraded surfaces, and release particles accumulated on the abraded surfaces. From the preliminary results, the following main findings and recommendations can be made.

1. The Taber rotary abraser is suitable for abrading flooring coatings and interior paints containing nanoparticles and for generating release particles for physical and chemical characterization.
2. LSCM, in combination with image analysis, is a good, relatively fast method for quantifying the number and size distribution of release particles accumulated on abraded surfaces having particle size greater than 100 nm.
3. Although further studies are being carried out for confirmation, preliminary microscopic results suggests that some nanoparticles incorporated in the matrix are present on the surfaces of released particles.
4. Commercial abrading wheels that are composed of a polymer matrix and inorganic abrasives typically used for evaluating the abrasion resistance of coatings and paints release particles may not be suited for use to generate release particles from nano-filled coatings and paints.
5. Wheels made of hard metal that do not release particles themselves should be used for abrading nano-filled coatings and paints. NIST is investigating metal material and wheel surface texture on the release particles.
6. One should be careful to consider the effect of abrading cycle on the number or size distribution of release particles accumulated on the abraded surface, because the repeated abrasion action on the specimen surface strongly influences the number or/and distribution of surface release particles.

****Disclaimer:** *Certain commercial product or equipment is described in this report in order to specify adequately the experimental procedure. In no case does such identification imply recommendation or endorsement by the National Institute of Standards and Technology, nor does it imply that it is necessarily the best available for the purpose.*

6. References.

1. Nanomaterials in plastics and advanced polymers, Market Report # 52, April, 2012, Future Markets, Inc.
2. T. McNally and P. Pötschke, Eds., Polymer-carbon nanotube composites, preparation, properties, and applications, Woodhead Publishing, Philadelphia, 2011.
3. J. R. Potts, D. R. Dreyer, C. W. Bielawski, R. S. Ruoff, Graphene-based polymer nanocomposites, Polymer, 52 (2011) 5-25.
4. B. Li and W.H. Zhong, Review on polymer/graphite nanoplatelet nanocomposites, J. Mat. Sci., 46 (2011) 5595-5614.

5. S. Pavlidou and C.D. Papaspyrides, A review on polymer-layered silicate nanocomposites, Progress in Polymer Science, 33 (2008) 1119-1198.
6. H. Zou, S.S. Wu, and J. Shen, Polymer/silica nanocomposites: preparation, characterization, properties, and applications, Chemical Reviews, 108 (2008)3 893-3957.
7. R. McIntire, Common nano-materials and their uses in real world applications, Science Progress, Vol. 95, no. 1.
8. Nanotechnology market forecast to 2013, Report by ResearchandMarkets, http://www. researchandmarkets.com/research/2012b4/nanotechnology_mar
9. M. Moukwa, Fascinating technology advances on the anvil in coatings industry, Chemical Industry Digest, January, 2011.
10. http://www.researchandmarkets.com/reportinfo.asp?report_id=1824738&t=t
11. R. McMullin, Manager, Nanotechnology, BYK North America, Private communication.
12. A. Nel, T. Xia, L. Mädler, N. Li, Toxic potential of materials at the nanolevel, Science, 311, 622-627 (2006).
13. C. Poland, et al., Carbon nanotubes introduced into the abdominal cavity of mice show asbestos-like pathogenicity in a pilot study, Nature Nanotechnology, 3 (2008) 423-428.
14. A.D. Maynard, Nanotechnology: Assessing the risks, Nanotoday, 2: 22-33 (2006).
15. K. Aschberger, et al., Review of carbon nanotubes toxicity and exposure – Appraisal of human health risk assessment based on open literature, Critical Reviews in Toxicology, 40(9) (2010): 759-790.
16. R.D. Handy, T.B. Henry, T.M. Scown, B.D. Johnston, and C.R. Tyler, Manufactured nanoparticles: Their uptake and effects on fish-A mechanistic analysis, Ecotoxicology 17 (2008) 396–409.
17. J. Lee, S. Mahendra, and P.J. Alvarez, Nanomaterials in the construction Industry: A review of their applications and environmental health and safety considerations, ACSNano, 4 (2010) 3580-3589.
18. A. R. Köhler, C. Som, A. Helland̲a, and F. Gottschalk, Studying the potential release of carbon nanotubes throughout the application life cycle, J. Cleaner Prod., 16 (2008) 927-937.
19. B. Nowack, et al., Potential scenarios for nanomaterial release and subsequent alteration in the environment, Env. Toxicol. Chem., 31 (2012) 50-59.

20. W. Wohlleben, et al., On the life cycle of nanocomposites: comparing released fragments and their in-vitro hazards from three release mechanims and four nanocomposites, Small, 7 (2011) 2384–2395.
21. L. Schlagenhauf, T.T. Bryan, B. Chu, J. Buha, F. Nüesch, and J. Wang, Release of carbon nanotubes from an epoxy-based nanocomposite during an abrasion process, *Environ. Sci. Technol.*, Accepted Manuscript, DOI: 10.1021/es300320y, Publication Date (Web): 04 Jun 2012.
22. L. Golanski, A. Guiot, and F. Tardif, New method for the characterization of abrasion-induced nanoparticle release into air from nanomaterials, Nanotech 2010, Anaheim, CA.
23. D. Bello, et. al., Exposure to nanoscale particles and fibers during machining of hybrid advanced composites containing carbon nanotubes. J. Nanopart. Res., 2009, 11, 231-249.
24. D. Bello, et al., Characterization of exposures to nanoscale particles and fibers during solid core drilling of hybrid carbon nanotube advanced composites. Int. J. Occup. Envir. Health, 2010, 16(4), 434-450.
25. D. Gohler, M. Stintz, L. Hillemann, and M. Vorbau, Characterization of nanoparticle release from surface coatings by the simulation of a sanding process. Ann. Occup. Hyg., 54 (2010) 615-624.
26. M. Vorbau, L. Hillemann, L. and M. Stintz, Method for the characterization of the abrasion induced nanoparticle release into air from surface coatings, J. Aerosol Sci., 40 (2009) 209-217.
27. L. Golanski, A. Gaborieau, A. Guiot, G. Uzu, J. Chatenet, and F. Tardif, Characterization of abrasion-induced nanoparticle release from paints into liquids, J. Phys. Conf. Ser. 304 (2011) 012062.
28. S. Sachse, et al., The effect of nanoclay on dust generation during drilling of PA6 nanocomposites, J. Nanomaterials, 2012, DOI10.151155/2012/189386.
29. E.J. Petersen, et al., Potential release pathways, environmental fate, and ecological risks of carbon nanotubes (critical review). Environ. Sci. Technol. 2011, 1-20.
30. L. Sung, J. Jasmin, X. Gu, T. Nguyen, J.W. Martin, Use of laser scanning confocal microscopy for characterizing changes in film thickness and local surface morphology of UV exposed polymer coatings. J. Coat. Technol. Res. 1 (2004) 267-276.
31. The NIH freeware *ImageJ* developed by National Institutes of Health (NIH) can be downloaded from http://rsb.info.nih.gov/ij/.

32. T. Nguyen, et. al., Degradation modes of crosslinked coatings exposed to photolytic environment, J. Coatings Technol. Res., in press, 2012.

Acknowledgments

The authors gratefully acknowledge project funding provided by the Consumer Products Safety Commission (CPSC) and valuable suggestions and comments by Dr. Treye Thomas of CPSC, as well as the assistances of the following NIST staff for various measurements: Drs. Lee Yu and Savelas Rabb for ICP-MS, Dr. Keana Scott for SEM, Dr. Justin Gorham for XPS, and Dr. Xiaohong Gu for AFM, Mr. Eric Byrd, Mr. John Hettenhouse, and Miss Debbie Stanley for abrasion instrumentation and specimen fabrication.